The new IPSL climate system model: IPSL-CM4

Olivier Marti, Pascale Braconnot, Jacques Bellier, Rachid Benshila, Sandrine Bony, Patrick Brockmann, Patricia Cadule, Arnaud Caubel, Sébastien Denvil, Jean-Louis Dufresne, et al.

The new IPSL climate system model: IPSL-CM4

Note du Pôle de Modélisation n°26

Marti O., P. Braconnot, J. Bellier, R. Benshila, S. Bony, P. Brockmann, P. Cadule, A. Caubel, S. Denvil, J.-L. Dufresne, L. Fairhead, M.-A. Filiberti, M.-A. Foujols, T. Fichefet, P. Friedlingstein, H. Gosse, J.-Y. Grandpeix, F. Hourdin, G. Krinner, C. Lévy, G. Madec, I. Musat, N. de Noblet, J. Polcher and C. Talandier

Institut Pierre Simon Laplace des Sciences de l'Environnement Global
IPSL Global Climate Modeling Group

June 7, 2006

IPSL
Case 101
4 place Jussieu
F75252 Paris Cedex 5
France

contact: olivier.marti@cea.fr

Contents

Chapter 1

Introduction

The estimate of future climate change and of its impact on the environment requires to increase our knowledge of the complex interactions between the atmosphere, the ocean, sea-ice, land surfaces and glaciers. These components are coupled through the cycles of energy and water, but also through biogeochemical cycles such as the carbon or the ozone cycles. One of the goals of the *IPSL* modeling community is to study how these different couplings can modulate climate and climate variability, and to determine how feedbacks in the Earth system control the response of climate to a perturbation such as the anthropogenic emissions of greenhouse gases. For this purpose, the Earth system model of the *IPSL* is developed as a modular suite of model components of the Earth system that can be use either as stand alone models or coupled to each other.

This note presents the new features and results of the last version of the global *IPSL* coupled model that will be used to run the set of simulations planned for the next *IPCC* assessment. In particular, chapter 2 presents the model components of the coupled system, highlighting important features for the coupling or the quality of model simulations. Chapter 3 synthesise all the coupling procedures and the coupling environment, and chapter 4 discussed the major characteristics of the model climatology.

1.1   The *IPSL* Earth system model: background

The *IPSL* "Earth system model" builds on all model developments achieved in four of the *IPSL* laboratories, *LMD*, *LODYC*, *LSCE*, *SA*, and from collaborations with *LGGE* for the high latitudes climate, *LOA* for the modeling of direct and indirect effects of the aerosols, *UCL/ASTR* for the new version of the sea-ice model, and *CERFACS* for the coupler. Successive versions of the global coupled model have been developed since 1995. They benefit from interactions within the GASTON group, created at that time to favor technical exchanges between French groups in Toulouse and Paris working on ocean-atmosphere coupled simulation. First simulations allowing for analyses of future climate change were available in 1998 (*Barthelet*, 1998).

Since the first version of the coupled model, the goals were to have a global coupled model, with no flux correction at the air sea interface that can be used to study present, future and past climates. The first version of the model (*Braconnot*, 1997) coupled the *LMD5.3* version of the *LMD* atmospheric model, with the *OPA 7* version of the ocean model developed at *LODYC*. In this version the sea-ice component was very simple and not realistic. Sea-ice appeared when temperature was below a threshold, and temperature and heat fluxes where estimated by the atmospheric model using the assumption that sea-ice was 3 meter thick. The *OASIS 2.2* coupler developed at *CERFACS* (*Terray et al.*, 1995) was used to synchronize the different models and for the interpolation of the coupling fields between the atmosphere and ocean grids. Sea surface temperature and sea-ice cover were interpolated using the four nearest neighbourgs. Heat fluxes and windstresses were interpolated using bicubic interpolation. In contrast to what was done in several modeling groups (cf. Stouffer, http://www.clivar.org/publications/wg_reports/wgcm/wgcm1_app.html), initial spin up adjustment was very simple. Ocean started from rest with temperature and salinity set to the values of *Levitus*

(1982) atlas in January. The initial state for the atmosphere was also January 1st of a forced ten year simulation.

The first simulations exhibited a large drift in surface air temperature, which has been attributed to an energetic imbalance of the atmospheric model, and, in particular, to the lack of low stratus clouds in mid-latitudes, as it was already found in an earlier version of the atmospheric model (*Bony and Le Treut*, 1992). Several adjustments were performed (*Braconnot*, 1998). A first set of modifications consisted in a better representation of the atmosphere boundary layer over mixed sea-ice and ocean grid cells. In the revised version, the fluxes were computed separately over each sub surface and then agregated to compute the temperature of the first atmospheric level. However, only the average surface flux was interpolated on the ocean grid (*LeClainche*, 2000). The second set of modifications was designed to equilibrate the atmospheric model. These changes concerned the threshold for vertical diffusion in stable cases, which allow for better simulation of temperature inversion in high latitude (*Krinner et al.*, 1997). This change had some interesting feedback on the tropical circulation by canceling the tendency of the model for super greenhouse effect (*Braconnot*, 1997). The drag coefficient was also adjusted in stable cases to allow for more exchange between the first layer of the atmospheric model and the surface. The balance between long wave and short wave radiation at the top of the atmosphere was achieved through the reduction of the water droplet size from $15\mu m$ to $8\mu m$, within the limits of available observations. However, although these adjustments allow stable coupled simulations, the energy absorbed in the tropical region was underestimated, which explains the cold tropical bias in the tropics in all simulations using this version of the model (*Braconnot et al.*, 2000). Mid-latitudes experienced a reversed bias. These characteristics improved when a new version of the *Morcrette et al.* (1986) radiative scheme was implemented (Dufresne and Fairhead, personnal communication). The hydrological cycle was also closed in this revised version, thanks to a simple routing scheme that considered the 46 major rivers (*Le Clainche*, 1996). Following the work of *Guilyardi et al.* (2001), isopycnal diffusion was implemented in the ocean model. A revised version of the interpolation scheme (3.3) also contributed to the conservation of energy at the air-sea interface.

The *IPSL_CM1* version of the coupled model was used to study the response of the coupled system to insolation (*Braconnot et al.*, 2000) and to the first simulations that considered both feedbacks from ocean and vegetation in past climate experiments from an asynchronous coupling with a biome model (*Braconnot et al.*, 1999; *Wohlfart et al.*, 2004). Several scenario experiments where the atmospheric concentration in CO_2 was increase were also performed and have been used as a basis to study decadal variability (*Laurent*, 2000).

The next step of the model development consisted to implement the complex *IPSL* thermodynamic sea ice model (*L'Heveder*, 1999; *Filiberti et al.*, 2001). This required some adjustment in the coupling procedure. In particular, in this *IPSL_CM2* version, the sea-ice model computed sea-ice albedo, and other surface parameters. Details of the coupling procedures can be found in *LeClainche* (2000). In addition, to insure the stability of the coupling over sea-ice, the derivative of the fluxes to temperature was also provided to the sea-ice model following the detailed stability analysis of *Dufresne and Grandpeix* (1996). With these changes, sea-ice was realistically simulated in the Arctic, and the overturning circulation in the Atlantic ocean better reproduced (*Le Clainche et al.*, 2001). Over the Antarctic ocean a fresh water input, mimicking the ice stream from the Antarctic ice sheet, was needed to maintain the sea ice cover. For this version, the spin up procedure consisted in running the coupled model for 10 years with a restoring term towards sea-surface-temperature climatology to initialize the sea-ice cover. The restoring term was then switched off afterwards.

The largest set of experiments with this *IPSL_CM2* version of the model concerned the first attempt to coupled a climate model and the carbon cycle (*Dufresne et al.*, 2002; *Friedlingstein et al.*, 2001). This was achieved in simulations where the coupled ocean-atmosphere model was asynchronously coupled to biochemical models of the vegetation and the ocean that computed carbon fluxes with the atmosphere. These simulations were analyzed to understand the strength of the coupling between climate and the carbon cycle (*Friedlingstein et al.*, 2003), and the impact of the climate change on the marine biota (*Bopp et al.*, 2001, 2003) or on the terrestrial biosphere (*Berthelot et al.*, 2002). This version of the model was also used to produce the first simulation showing how changes in the ocean could have trigger the last glacial inception (*Khodri et al.*, 2001), and to discuss how precession impact the mean seasonal cycle of climate and the monsoon phenomenon from several sensitivity experiments to precession (*Braconnot and Marti*, 2003).

6

VERSION (reference)	CHARACTERISTICS	MAIN STUDIES	INTERNAT. PROJECTS	DATA DIFFUSION AND OTHER STUDIES
IPSL_CM0 (*Braconnot*, 1997)	Atm: LMD5.3. Ocean: OPA7. Sea-ice: `IF` or restoring to climatology. Land-surface:Sechiba. Coupler: OASIS.	Global change scenarii (*Barthelet*, 1998)		
IPSL_CM1 (*Braconnot et al.*, 2000)	Atm: LMD5.3 with fractionnal sea-ice and ocean boxes and boundary. Adjustments: droplet size, minimum vertical diffusivity, ice water transition, radition scheme. Ocean: OPA7. Sea-ice: `IF` or restoring to climatology. Land-surface: Sechiba. Coupler: OASIS.	Global change scenarii. Interannual and decadal variability (*Laurent*, 2000). Climate of the mid-Holocene (*Braconnot et al.*, 2000). Ocean-atmosphere-vegetation coupling during the Mid-Holocene (*Braconnot et al.*, 1999; *Wohlfart et al.*, 2004)	CMIP. ENSIP (*Latif et al.*, 2001), STOIC (*Davey et al.*, 2002). PMIP: working group and coupled simulations (WCRP-111, WMO/TD-No. 1007; *Braconnot et al.*, 2000, 2004; *Zhao et al.*, 2005)	ECHO (PNEDC project), PMIP : Model outputs used by several groups (Cérège, University of Bristol, University of Saõ Paolo, Max Planck Institüte Jena).
IPSL_CM2 (*Le Clainche et al.*, 2001)	Atm: LMD5.3 (same as IPSL_CM1). Ocean: OPA7. Sea-ice IGLOO thermodynamic model. Land-surface: Sechiba.	Sea-ice feedbacks (*LeClainche*, 2000). Glacial inception (*Khodri et al.*, 2001). Climate sensitivity to precession (*Braconnot and Marti*, 2003). Climate-carbon coupling (*Dufresne et al.*, 2002; **?**; *Friedlingstein et al.*, 2003; *Berthelot et al.*, 2002)	CMIP (*IPCC*, 2001)	CLIMPACT

Table 1.1: A brief history of the IPSL climate model - 1

VERSION (reference)	CHARACTERISTICS	MAIN STUDIES	INTERNAT. PROJECTS	DATA DIFFUSION AND OTHER STUDIES
IPSL_CM3 (*Li and Conil*, 2003)	Atm: LDMZ.3. Ocean: OPA8. Sea-ice: restoring. Land-surface: bucket			
IPSL_CM4	Atm: LMDZ.3 with Emanuel convection scheme, new cloud scheme, adjustments of ocean albedo, adjustments of minimum vertical diffusivity. Ocean: OPA8.5 Sea-ice: LIM (Louvain Ice Model). Land-surface: ORCHIDEE.			

Table 1.2: A brief history of the IPSL climate model - 2

1.2 New features for version *IPSL_CM4*

Interesting results have been obtained with the *IPSL_CM2* version of the model. However some biases in the model climatology needed to be corrected. Increased interest for mid and high latitude climate leads also to the need for a better resolution at high latitudes. Due to the cold bias of the model in the tropics, several aspects of the tropical interannual variability needed improvement. Moreover the computing center changed respectively from *Crays* to *VPP* and *NEC*, which required to adapt several aspects of the codes and coupling procedures. New versions of the different model components (ocean, atmosphere, land surface and sea-ice) were also ready and became the basis for new developments.

The assembly of these new components and a complete revision of the coupling scheme was undertaken. A first version of the coupling between the *LMDZ* model and *ORCA* leads to a 1000 years simulation (*Li and Conil*, 2003). This *IPSL_CM3* version of the model was developed to study interannual variability in the tropics. The land surface scheme and sea-ice models were not included. However the development of the *IPSL_CM4* version benefits from all the work done in the rewriting of the boundary layer of the model that allowed for different sub surfaces in a grid cell, following *Grenier* (1997).

As for previous versions, the objective was to have a version with no flux correction at the air-sea interface and no major drift in climate characteristics that can be integrated for several centuries. The closure of the energetic and the water cycle was at the heart of the efforts. Model development were performed so that the model can be used both to study climate change and climate variability. Specific care was thus given to the large scale characteristics of climate, including the land-sea contrasts, the gradients between equator and poles, and some aspects of the interannual variability such as the ENSO signal. These criteria have been mainly fulfilled thanks to new physical parameterizations and adjustments of the radiative forcings in the atmospheric component. The model should also be easy used by a wide variety of users, which pushes us to develop common a common model environment. At the moment two resolutions of the model are available: LMDZ 72x45x19 / ORCA 92x76x31 and LMDZ 96x72x19 / ORCA 182x149x31. The different aspects of the model development are described in the remainder of this document. They concerned:

- The *ORCA-LIM* coupling.

  The Louvain-la-Neuve sea ice model *LIM* (*Fichefet and Morales Maqueda*, 1997) has been introduced and coupled to the ocean model *OPA*, for which the *ORCA* grid definition is used (see section 2.4).

- Sub-surfaces in LMDZ and interface routines.

  In order to get the same coastline between the ocean and the atmosphere models, each atmospheric grid cell is divided into four sub surfaces, ocean, sea-ice, glacier and land. The boundary layer of the atmosphere model has been rewritten to solve the vertical diffusion on the different sub-grid cells. At the interface, the physical consistency and energy conservation is achieved through the sum of the fluxes exchanged with each sub surface. In addition an interface model has been introduced in the atmosphere model. It allows for an easy switch on or off of the different subsurface components and a better definition of the coupling fields between them.

- LMDZ - ORCHIDEE coupling.

  The work done on the atmosphere boudary layer allow for a coupling between the *LMDZ* and the new version of the *IPSL* land surface scheme *ORCHIDEE* (*Krinner et al.*, 2005) that follows the recommendation of the *PILPS* interface (*Polcher et al.*, 1998). A routine scheme has also been introduced in the land surface scheme, which allows to close the hydrology budget.

- New Interpolation scheme.

  The interpolation scheme between the ocean and the atmosphere grids has been revised. The new schemes ensure both a global and local conservation of the different fluxes at the air-sea interface thanks to the common coastline between the two models. A distinction is also made between ocean and sea-ice fluxes.

- New environnement

  Since the model and its components can be used for different applications and by a wide range of users, it becomes more and more important that they all share the same computing environment while keeping a large flexibility for the model setting. Model releases need also be easily available and documented. To meet these requirements, the model benefits from a user friendly computing environment. All models use the same library based on the NetCDF format, *IOIPSL*, for input/output. Source versions are maintained through CVS, and the computing environment (`modipsl`) allows for easy retrieval of a model versions and launch of reference simulations. Online monitoring and automatic atlases with basic diagnostics have also been implemented.

1.3 Electronic versions of this document

This documentation is available on line at http://igcmg.ipsl.jussieu.fr/Doc/IPSLCM4, as well as all scripts and data used to draw the figures. You will find there various formats:

- Web site, with color figures, navigation panel, etc ...;

- Printable PDF document, with black and white figures (most of them) and clickable internal and external links (approximatively 7 Mo).

- Printable PostScript document, with mostly black and white figures (approximatively 45 Mo) ;

- Printable PDF document , with color figures and clickable internal and external links (approximatively 7 Mo) - in construction ;

- Printable PostScript document, with color figures (approximatively 45 Mo) - in construction ;

- The original files are available here.

- The Ferret jnl files used to draw all figures are available here.

- All data used for this documentation are accessible through `http` or *OPenDAP/DODS* at http://dods.extra.cea.fr/data/p86mart/IPSL

Chapter 2

The components of the IPSLCM4 model

2.1 Introduction

The *IPSLCM4* model presently couples four components of the Earth system. *LMDZ* is the component for atmospheric dynamics and physics. *ORCA* is the component for ocean dynamics. *LIM* is the component for sea-ice dynamics and thermodynamics. *ORCHIDEE* handles the land surface.

p (hPa)	1004.	985.	956.	914.	852.	770.	667.	547.	422.
z (km)	0.078	0.250	0.500	0.880	1.46	2.01	3.47	5.04	7.01
311	233.	183.	140.	104.	72.	47.	27.	14.	3.0
9.19	11.2	12.7	14.4	16.2	18.4	21.0	24.7	28.7	40.1

Table 2.1: Vertical discretization (pressure in hPa and altitude in km) for the 19 layers of the *LMDZ* model over oceans.

2.2 The atmospheric component: LMDZ

The atmospheric component of the *IPSLCM4* model, *LMDZ*, is a classical atmospheric general circulation model, inherited from the original climate model of Laboratoire de Métérologie Dynamique (*Sadourny and Laval*, 1984). The model can be schematically presented as the coupling between a dynamical core and a set of physical parameterizations.

2.2.1 The 3D dynamical core

The dynamical part of the code is based on a finite-difference formulation of the primitive equations of meteorology developed by R. Sadourny (see e. g. *Sadourny and Laval*, 1984) and coded by P. Le Van. The global grid is stretchable in both longitude and latitude (the *Z* of *LMDZ* stands for Zoom). For the applications presented here, the grid is regular in both directions. The discretization insures numerical conservation of both enstrophy for barotropic flows and angular momentum for the axi-symetric component. Both vapor and liquid water are advected with a monotonic second order finite volume scheme (*Van Leer*, 1977; *Hourdin and Armengaud*, 1999). The time integration is done with a leapfrog scheme, with, periodically, a predictor/corrector time-step. The time step is bounded by a CFL criterion on the fastest gravity modes. For the current grids, with $72x45$ points for the low resoltution, or $96x72$ for the intermediate resolution, the time-step is of a few minutes. For latitudes poleward of $60°$ in both hemispheres, a longitudinal filter is applied in order to limit the effective resolution to that at $60°$..

An horizontal dissipation operator, aimed to represent the interaction with unresolved motions, is applied on both winds and temperature. This operator is based on an iterated laplatian, designed so as to represent properly the pumping of enstrophy (square of the wind curl) at the scale of the grid.

On the vertical, the model uses a classical hybrid $\sigma - p$ coordinate: the pressure P_l in layer l is defined as a function of surface pressure P_s as $P_l = A_l P_s + B_l$. The values of A_l and B_l are chosen in such a way that the $A_l P_s$ part dominates near the surface (where A_l reaches 1), so that the coordinate is following the surface topography (like so-called σ coordinates), and B_l dominates above several km, making the coordinate equivalent to a pressure coordinate there. The current version of the *IPSLCM4* model is based on 19 layers. Averaged values of pressure and altitude at half levels over oceans are given in table 2.1.

This dynamical code has been widely used not only for Earth but also for the numerical simulations of the general circulation of other planetary atmospheres, in particular for Mars (*Hourdin et al.*, 1993; *Forget et al.*, 1999) and Titan (*Hourdin et al.*, 1995).

2.2.2 The physical package

Coupled to the dynamical core, the model includes a set of physical parameterizations.

The radiation scheme is the one introduced several years ago in the model of European Centre for Medium-Range Weather Forecasts (*ECMWF*) by Morcrete: the solar part is a refined version of the scheme developed by *Fouquart and Bonnel* (1980) and the thermal infra-red part is due to *Morcrette et al.* (1986).

Turbulent transport in the planetary boundary layer is treated as a vertical diffusion with an eddy diffusivity depending on the local Richarson number (*Laval et al.*, 1981). The surface boundary layer is treated according to *Louis* (1979). A countergradient term is applied for potential temperature, and unstable profiles are prevented using a dry convective adjustment.

12

Condensation is parameterized separately for convective and non-convective clouds. Moist convection is treated using mass flux approaches Recently, during the preparation of the IPSLCM4 model, *Emanuel* (1991) scheme was adopted in place of *Tiedtke* (1989) scheme as discussed below. Clouds are represented through a probability distribution function of subgrid scale total (vapor and condensed) water (*Le Treut and Li*, 1991; *Bony and Emmanuel*, 2001). Effects of mountains (drag, lifting, gravity waves) are accounted for using a state-of-the-art schemes (*Lott and Miller*, 1997; *Lott*, 1999).

The dynamics and physics are clearly separated in the code and communicate through a well defined interface. The dynamical core is written in a 3D world whereas the physical package is coded as a juxtaposition of 1D columns. This allows to easily test the physical package in a single-column context. The physical parameterizations could also be easily used on a different spatial grid than dynamics, for example on the oceanic grid for a coupled model (delocalized physics as experienced by *Vintzileos et al.*, 1999).

2.2.3   Recent improvements

Convection

The most noticable improvement of the atmospheric component during the development phase of the *IPSLCM4* model has been the introduction of the *Emanuel* (1991) scheme in place of *Tiedtke* (1989) scheme. The version of Tiedtke scheme used at *LMD*, close to the original formulation, relies on a closure in moisture convergence (CISK mechanism). With this parameterization, *LMDZ* tends to systematically overestimate precipitation over oceanic areas in the tropics, in particular on the west side of the indian and pacific oceans The precipitation during the rain season on Africa and south America is also underestimated. The Emanuel scheme was chosen for the coupled model because it significantly improved the above mentioned deficiencies as seen in fig. 2.1 and fig. 2.2.

Clouds

Following the introduction of the new convection scheme, a significant effort was put on the cloud scheme. As in other GCMs, the cloud cover f and in-cloud water q_c are deduced from the large scale large scale total (vapor and condensed) water $\overline{q}$ and moisture at saturation, q_{sat}, using a Probablity Distribution Function (PDF) $P(q)$ for the subgrid-scale total water q:

$$f = \int_{q_{\text{sat}}}^{\infty} P(q)dq \quad \text{and} \quad q_c = \int_{q_{\text{sat}}}^{\infty} (q - q_{\text{sat}})P(q)dq \tag{2.1}$$

In the original formulation *Le Treut and Li* (1991), the subgrid scale distribution of total water is described throug a top hat distribution of width $\sigma = r\overline{q}$ around $\overline{q}$ where the ratio r is an imposed parameter (a decreasing function of pressure in *LMDZ*).

Following *Bony and Emmanuel* (2001), the top-hat function has been replaced recently by a generalized log-normal function bounded to zero (fig. 2.4). The distribution depends also on one width parameter only. The distribution tends to a gaussian distribution when the ratio r tends to zero. Because it is bounded at zero, the distribution shows a skewness toward large values. This skewness increases with r as observed in the mid troposphere in convective region (strong convection being asscociated with both a large dispersion of humidities and a large skewness).

Even with this improved PDFs, the parametrization with a unique function r of pressure is not sufficient to real-istically predict the contrast between strongly convective clouds in a rather dry troposphere and more homogeneous conditions. A special treatment is thus applied for convective clouds.

For the previous version of the model, based on Tiedtke scheme, the convective cloud cover is imposed as a function of the total convective rain-fall at the surface (after Slingo, personal communication). For the tests presented here, this approach is refined further by using as a predictor, instead of the surface rainfall, minus the vertical integral of the negative tendency of total water, associated to convection. Both predictors are identical for strongly precipitating systems but the second one allows to obtain a much more realistic cloud cover for regions of non precipitating cumulus clouds.
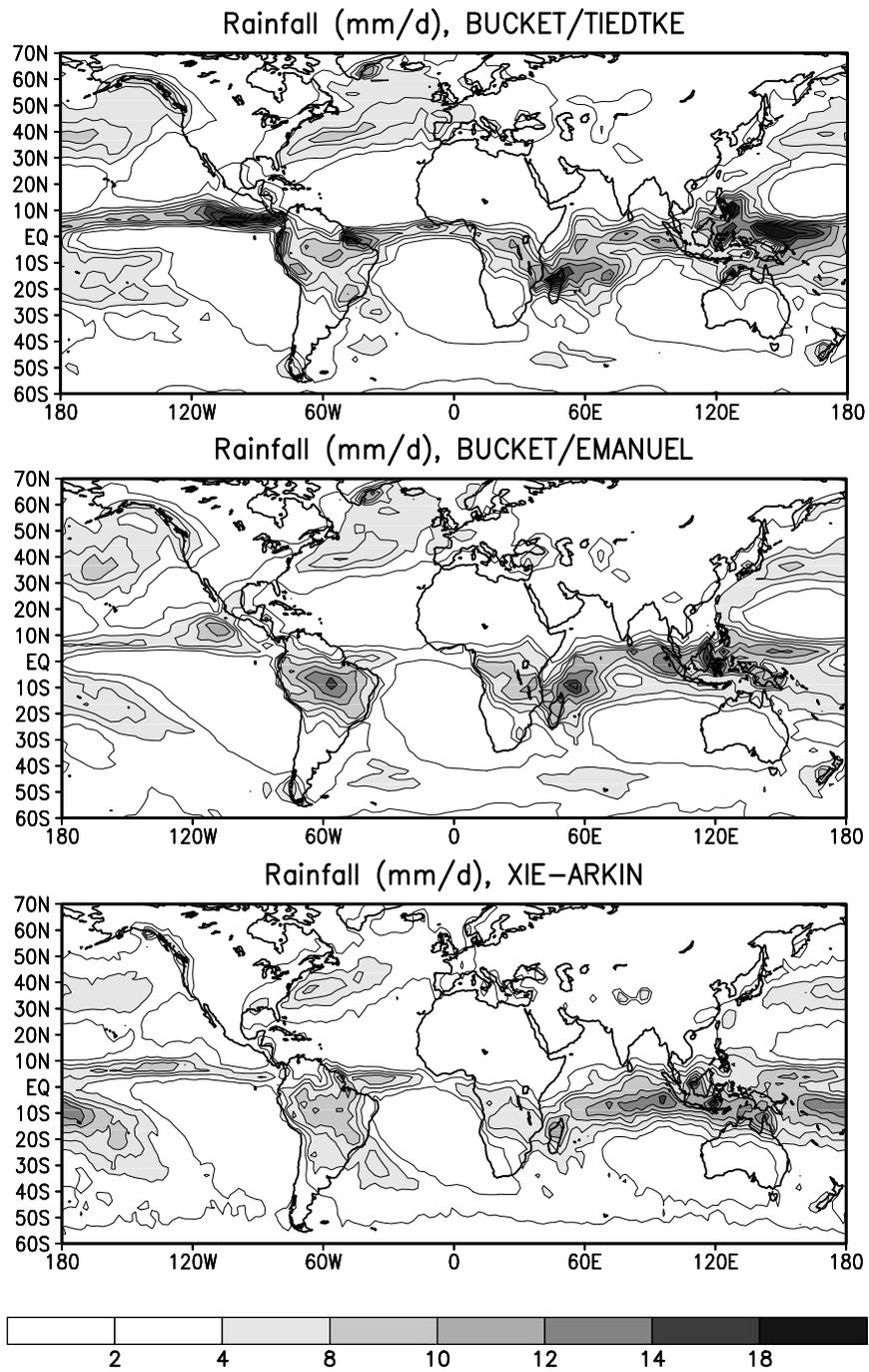
Figure 2.1: January rainfall (mm/day) for a six-year simulation with climatological sea surface temperature. The top panel correspond to Tiedtke convection scheme, the mid panel to Emanuel scheme and the bottom one to CMAP data.

Rainfall (mm/d), BUCKET/TIEDTKE

**Rainfall (mm/d), BUCKET/EMANUEL**

Rainfall (mm/d), XIE−ARKIN
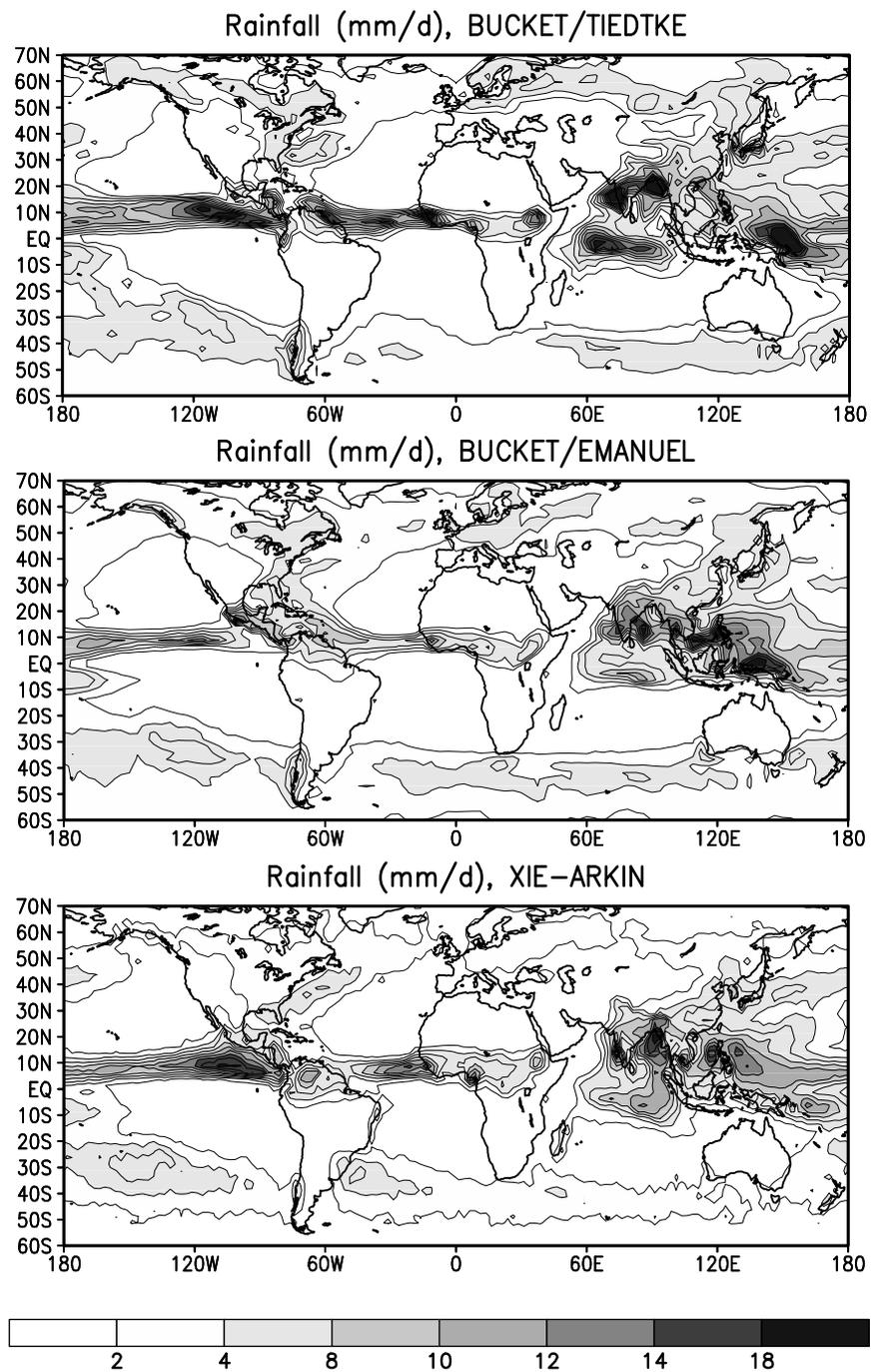
Figure 2.2: July rainfall (mm/day) for a six-year simulation with climatological sea surface temperature. The top panel correspond to Tiedtke convection scheme, the mid panel to Emanuel scheme and the bottom one to CMAP data.

CRFSW, BUCKET/TIEDTKE

CRFSW, BUCKET/EMANUEL

CRFSW, ERBE
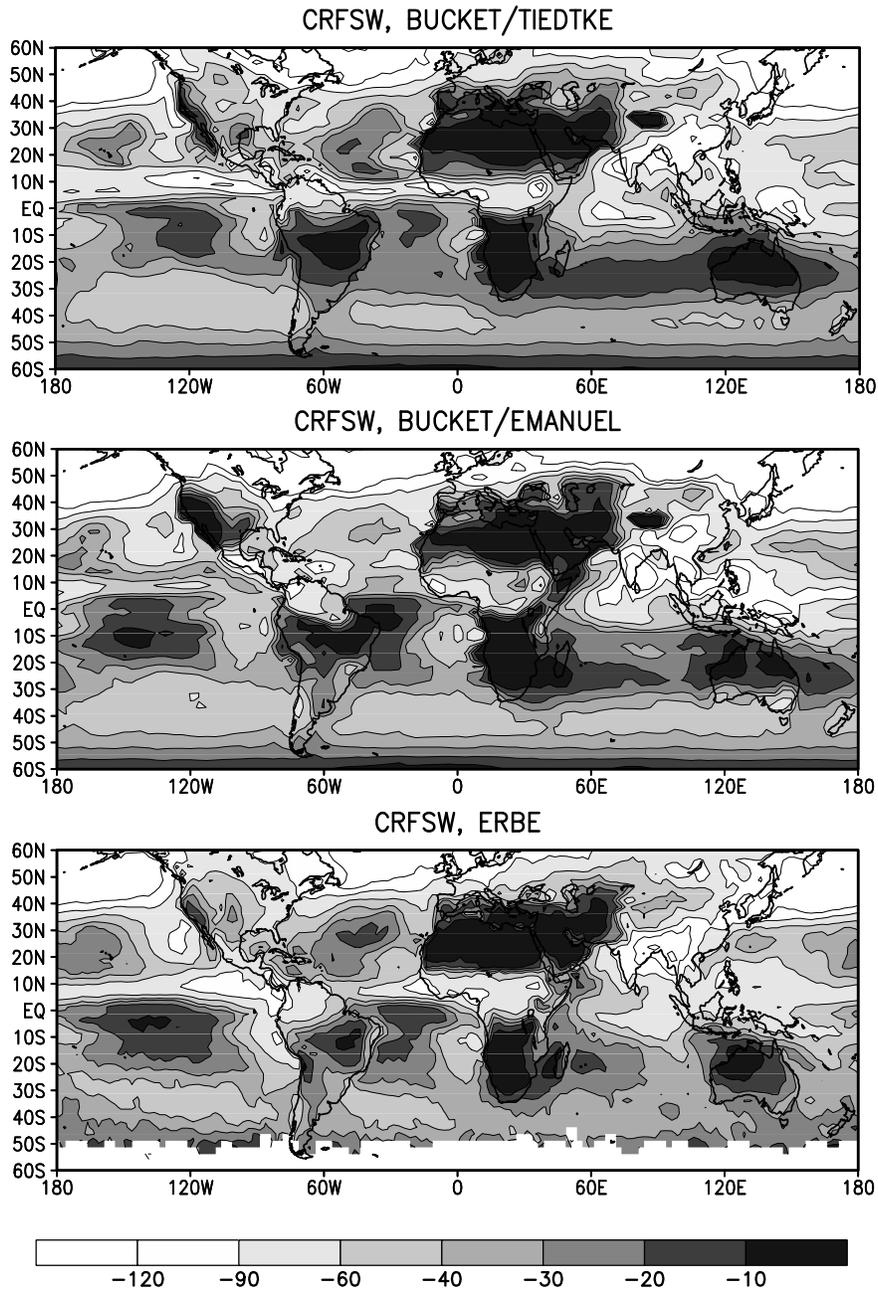
Figure 2.3: July short-wave cloud radiative forcing (W/m^2) for a six-year simulation with climatological sea surface temperature. The top panel correspond to Tiedtke convection scheme, the mid panel to Emanuel scheme and the bottom ones to *ERBE* data.
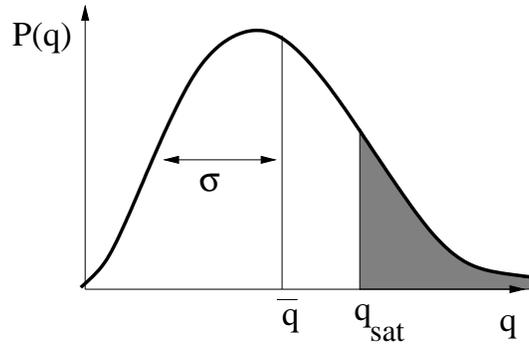
Figure 2.4: Probability Distribution Function of water.

For the Emanuel scheme, we adopted a more consistent approach proposed by *Bony and Emmanuel* (2001). In this approach, r is estimated in each convective mesh from an inverse procedure, so as to obtained the incloud condensed water predicted by the convection scheme.

As an illustration, we show in fig. 2.3 the short-wave cloud radiative forcing (difference of the total and clear-sky short-wave radiation at the top of the atmosphere) for both simulations in July. In both version, the overall range of the radiative forcing is well represented. The spatial distribution of clouds in the tropics is of course affected by the errors in the distribution of convective rainfalls. Note that the longitudinal contrast in the oceanic bassin, with a stronger radiative forcing on the east side (both at $0°$-$20°$S on the three oceans and at $10°$-$30°$N on the pacific) is rather well represented. This behavior, associated to the contrast between trade wind cumulus and strato-cumulus on the east basins of tropical oceans is obtained thanks to a dependency of the threshold (minimum) value of the turbulent viscosity on the strength of the inversion at the top of the boundary layer. The introduction of the Emanuel scheme and the adjustment of the cloud radiative forcing for coupling, have required a significant work on the cloud scheme.

Tuning of the boundary layer scheme

The formulation of the boundary layer is very sensitive of the minimum diffusivity in high latitudes. Specific care was given to this threshold in order to get the right strength of the polar inversion following the work done by *Krinner et al.* (1997) and *Grenier et al.* (2000). It was also shown with the *LMD5* version of the *LMD* model, that this simple tuning was necessary to get the right temperature profils over sea-ice *Braconnot* (1998).

The formulation of the drag coefficient over the ocean was also revisited. In its original version the surface roughness length over the ocean follows Charnock's formula. The neutral drag coefficient was prescribed to 10^{-3}. The stability functions are those of *Louis* (1979). Under unstable conditions over the ocean the empirical interpolation of *Miller et al.* (1992) is used between the free convection limit and the neutral approximation.

In the new version the formulation of *Smith* (1988) was introduced to compute the surface roughness length. For practical reason, the differentiation between heat and momentum drag coefficient was achieved by prescribing a 0.8 factor between the respective neutral drag coefficients, which roughly mimics the difference in *Smith* (1988) neutral drag coefficient between heat and momentum in moderate to high wind speed. Several sensitivity experiments showed that this factor is important to control the evaporation in subtropics and the advection of moisture in the low level branch of the Hadley circulation. Precipitation over the Pacific warm pool is sensitive to this parameter.

Another major source of improvement is the hydrological scheme (see 2.3.3).

Coupling with sub-surfaces

For coupling purposes, a fractional land-sea mask was introduced in the model. Each grid box was then divided into four sub-surfaces corresponding to land surface, free ocean, sea-ice and glaciers. Surface fluxes are computed using parameters (roughness length, albedo, temperature, humidity etc..) adapted to each surface type. For each atmospheric

column, vertical diffusion is applied independently for each sub-surface, and the resulting tendencies are averaged. In addition an interface model was also introduced to disconnect more easily surface processes from the atmosphere. The diffusion scheme was rewritten to systematically force the boundary layer by surface fluxes. The computation of surface fluxes is done in an independent model which requires providing this model with the sensitivity of the turbulent flux to temperature, in order to preserve the properties of the semi-implicit scheme. With this formulation the flux model can be either a routine in the atmospheric model, an ocean model or a land surface scheme.

2.3 The land surface model ORCHIDEE

2.3.1 The three components of the land surface model

ORCHIDEE is divided is three modules, two based on existing models and one newly developed (*Krinner et al.*, 2005).

1. The hydrological module *SECHIBA* (*Ducoudré et al.*, 1993) which has been developed as a set of surface parameterizations for an atmospheric general circulation models. *SECHIBA* describes the short-timescale processes (of the order of a few minutes to hours) of energy and water exchanges between the atmosphere and the biosphere. The parameterizations of photosynthesis follows *Farquhar et al.* (1980) for C_3 plants and *Collatz et al.* (1992) for C_4 plants. Stomatal conductance is calculated following *Ball et al.* (1987). Time step of the hydrological module is of the order of 30 minutes.

2. The parameterizations of vegetation dynamics: fire, sampling establishment, light competition, tree mortality, and climatic criteria for the introduction or elimination of plant functional types. These parameterizations have been taken from the dynamic global vegetation model *LPJ* (*Sitch et al.*, 2003). The effective time step of the vegetation dynamics parameterizations is one year.

3. The other processes such as carbon allocation, litter decomposition, soil carbon dynamics, maintenance and growth respiration, and phenology form together a third module called *STOMATE*. This module essentially simulates the carbon dynamics of the terrestrial biosphere. Treating processes that can be described on time scales of a few days (time step is one day). This module calculates plant phenology, based on the previous work of *Botta et al.* (2000), autotrophic respiration, based on *Ruimy et al.* (1996), carbon allocation based on *Friedlingstein et al.* (1999), and autothropic respiration, using a litter ans soil carbon module derived from the *CENTURY* model (*Parton et al.*, 1988). *STOMATE* is the link between the fast hydrological processes of *SECHIBA* and the slow processes of vegetation dynamics described by *LPJ*.

ORCHIDEE can be run in different configurations, depending on the type of problem to be addressed. These are:

1. Hydrology only. In this case, *STOMATE* is entirely deactivated and leaf conductance is calculated as in *Ducoudré et al.* (1993) without using any parameterizations of photosynthesis. Vegetation distribution and leaf area index (LAI) are prescribed.

2. Hydrology and photosynthesis. In this case, the parameterizations of photosynthesis (following *Farquhar et al.* (1980) and *Collatz et al.* (1992)) and stomatal conductance (following *Ball et al.*, 1987) are activated, but vegetation distribution and LAI are still prescribed using satellite input data.

3. Hydrology and carbon cycle with static vegetation. In this case, the carbon cycle is fully activated. Soil, litter and vegetation carbon pools (including leaf mass and thus LAI) are prognostically calculated as a function of dynamic carbon allocation. However, the vegetation distribution is prescribed (*LPJ* is de-activated).

4. Hydrology and carbon cycle with dynamic vegetation. In this case, *SECHIBA*, *STOMATE* and *LPJ* are fully activated and the model makes no use of satellite input data that would force the state of the vegetation, so that the leaf and vegetation cover, with their seasonal and interannual variability, are entirely simulated by the model.

In any of these configurations, *ORCHIDEE* can be run in stand-alone mode, that is, forced by climatological or experimental data (global or local), and it can be run coupled to *LMDZ*.

Like *LPJ*, from which the parameterizations of vegetation dynamics have been taken, *ORCHIDEE* builds on the concept of plant functional types (PFT) to describe vegetation distributions. This concept allows to group species with similar characteristics into functional types in ways which maximise the potential to predict accurately the responses of real vegetation with real species diversity.

ORCHIDEE distinguishes 12 PFTs: tropical broad-leaved evergreen trees, tropical broad-leaved raingreen trees, temperate needleleaf evergreen trees, temperate broad-leaved evergreen trees, temperate broad-leaved summergreen
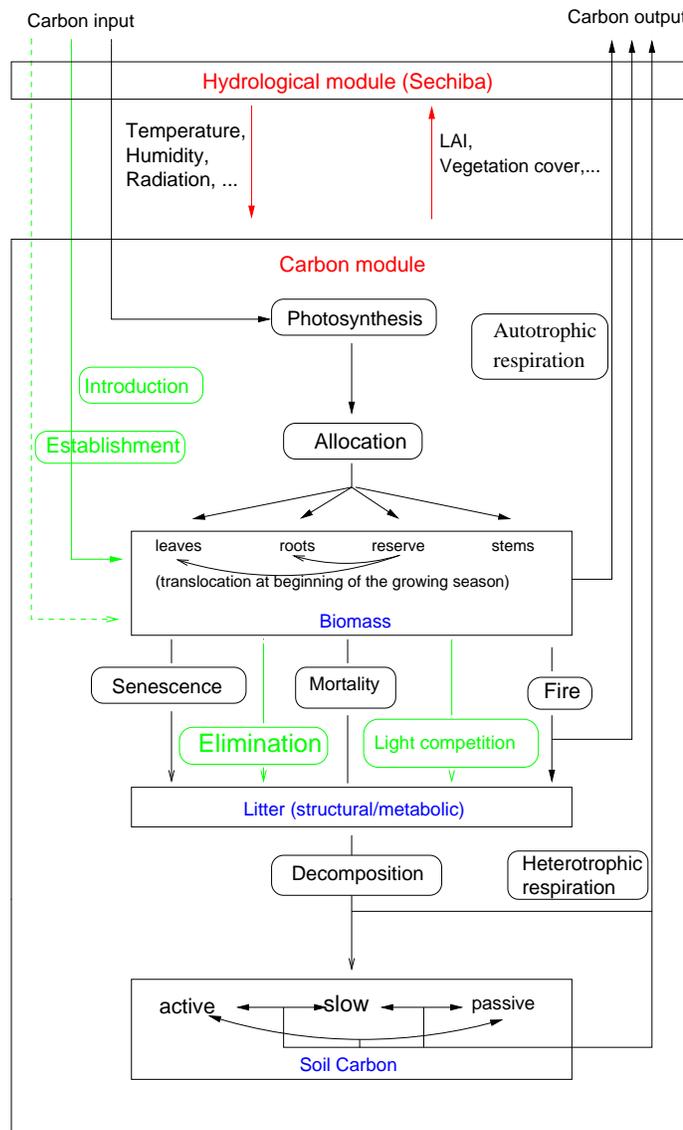
Figure 2.5: Basic structure of *ORCHIDEE*. Vegetation dynamics processes (taken from *LPJ*) show up in green. Within the carbon module box, processes are marked by rounded rectangles, while carbon reservoirs are indicated by normal rectangles (with the corresponding basic state variables in blue). The subprocesses simulated in the carbon module are linked trough carbon fluxes (black and green arrows). The exchange of energy and information with the atmosphere passes through the surface scheme (that is, the hydrological module).

trees, boreal needleleaf evergreen trees, boreal broad-leaved summergreen trees, boreal needleleaf summergreen trees, C_3 grass (natural and agricultural), and C_4 grass (natural and agricultural).

This set of PFTs is the same as that chosen in *LPJ*, plus the two agricultural PFTs. In every grid element the different PFTs can coexist, the fraction of the element occupied by each PFT being either calculated (and thus variable in time) or prescribed. The fractional area occupied by agricultural PFTs is always prescribed, *i.e.* vegetation dynamics does not act on the agricultural fraction of the grid element. Stomatal resistances are calculated separately for each PFT (and so is the resistance of bare soil). Water reservoirs are calculated for each PFT separately, but the reservoirs can be mixed using a prescribed time constant. This constant is generally chosen to be $\tau = 1$ day, which means that the different PFTs essentially dispose of the same quantity of water.

2.3.2 River routing

ORCHIDEE includes (in *SECHIBA*) an original routing scheme which combines the horizontal flow of water in the river basins with the vertical processes classically included in land-surface models. It is based on the work of *Hagemann and Dümenil* (1998), and uses a cascade of three reservoirs: the stream and two aquifer reservoirs, each being associated with only one time constant (fig. 2.6). In each grid-cell the runoff and drainage are the water supply of the routing system. Topography governs the water transport from one grid cell its neighbors, and more than one basin can be accounted for per grid box. Processes such as flood plains and irrigation are also parameterised (*De Rosnay et al.*, 2003). Of particular importance for coupled models is the fact that this approach allows to treat correctly endorehic basins. The water of these land-locked basins flows into lakes which can then re-evaporate. This water does not need to be distributed in some way over the ocean in order to satisfy the conservation equation.

It is important to note that while the surface processes affect the river routing through their influence on surface runoff and drainage, the routing scheme does not affect the land surface processes in *ORCHIDEE*: there is no evaporation from the rivers, and the aquifer reservoirs are not connected to the deep soil moisture as it is in the real world.

ORCHIDEE in this configuration has been validated over a wide range of regions and time scales and gives satisfactory results as discussed in *Verant et al.* (2003) and *Ngo-Duc et al.* (2005).

2.3.3 Impact of ORCHIDEE on atmospheric simulations

The surface scheme yields to a major improvement of atmospheric simulations. Although some older versions of the *LMD* model did include the thermodynamic model *SECHIBA*, until recently, the *LMDZ* was using a simple bucket model for the water budget on continental surfaces, following *Laval et al.* (1981). In this bucket version, thermal conduction in the soil is treated with a 11-layer discretization of the conduction equation for an homogeneus surface (*Hourdin et al.*, 1993).

Introduction of *ORCHIDEE* scheme results in two major improvements. The first one is a reduction of an irealistic maximum of precipitation in January over the west indian ocean, close to Madagascar. The second improvement is a reduction of summer precipitation over the continent of the northern hemisphere. Introduction of the *ORCHIDEE* has also some negative effects. The rainfall over the Amazone delta decreases. The rainfall over the middle of the indian sub-continent increases irealistically in July while the extension of the monsoon to the north-west is reduced.
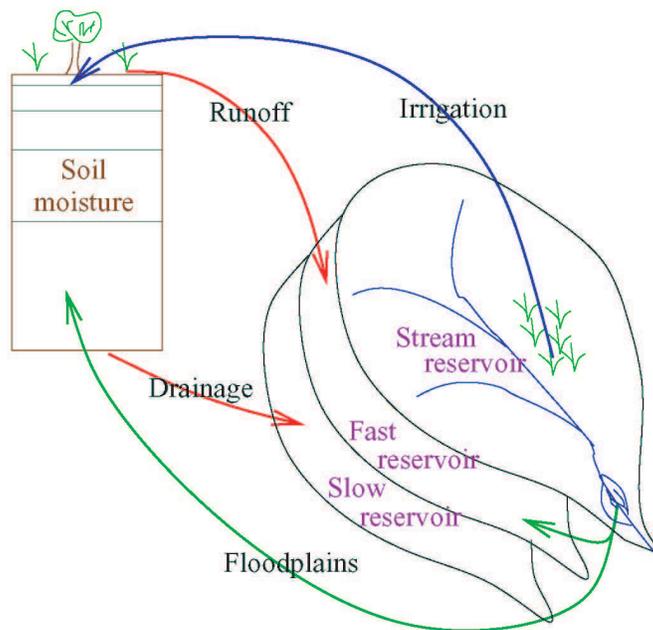
Figure 2.6: Schematic description of the routing scheme.
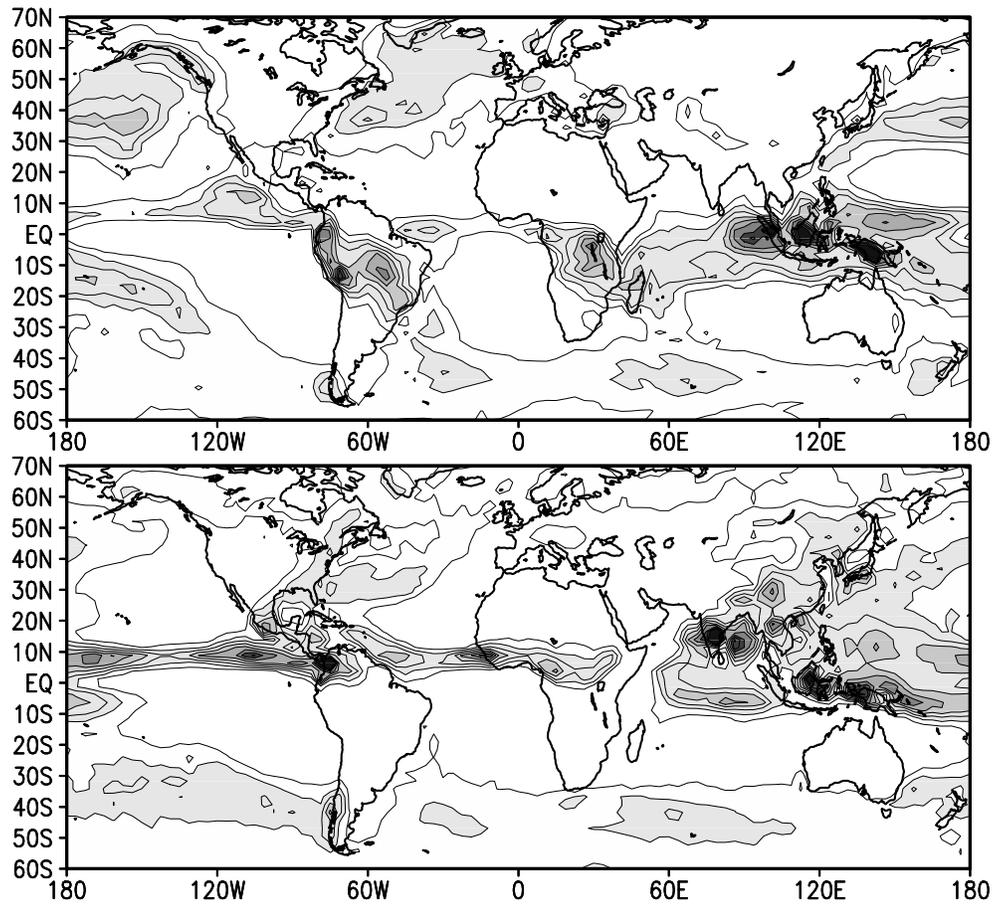
Figure 2.7: Mean rainfall (mm/day) for January (left) and July (right) for a six-year simulation with climatological sea surface temperature. The top panel correspond to Tiedtke convection scheme, the mid panel to Emanuel scheme and the bottom one to CMAP data.

2.4 The oceanic component: the OPA System

2.4.1 The OPA Oceanic General circulation model

The OPA system is a primitive equation model of both the regional and global ocean circulation. It is intended to be a flexible tool for studying ocean and its interactions with the others components of the Earth climate system (atmosphere, sea-ice, biogeochemical tracers, ...) over a wide range of space and time scale. Prognostic variables are the three-dimensional velocity field and the thermohaline variables. The distribution of variables is a three dimensional Arakawa-C-type grid using prescribed $z-$ or $s-$levels. Various physical choices are available to describe ocean physics, including a 1.5 turbulent closure for the vertical mixing. *OPA* is interfaced with a sea-ice model, a passive tracer model and, via the *OASIS* coupler, with several atmospheric general circulation models. In addition, it can be run on many different computers, including shared and distributed memory multiprocessor computers.

2.4.2 The 3D dynamical core

The ocean is a fluid which can be described to a good approximation by the primitive equations, *i.e.* the Navier-Stokes equations along with a non-linear equation of state which couples the two active tracers (temperature and salinity) to the fluid velocity, plus the following additional assumptions made from scale considerations: spherical Earth approximation; thin-shell approximation ; turbulent closure hypothesis; Boussinesq hypothesis; hydrostatic hypothesis; incompressibility hypothesis.

The primitive equations are written using a tensorial formalism so that any orthogonal curvilinear coordinate system which preserves the local vertical can be used.

The basic idea of numerical methods consists in discretizing differential equations on a three dimensional grid and computing the time evolution of each variable for each gridpoint. Ocean models are usually written in finite difference form. Such a method provides a legible computer code, easy to update, and is able to deal with the complex boundary conditions formed by the coastline geometry and the bottom topography.

The OPA reference manual describes in detail the ocean physics as taken in account by the model (explicitly or using sub-grid parametrization) as well as boundary conditions (surface, bottom, lateral), numerical schemes and computer implementation.

2.4.3 The configurations used in IPSLCM4: ORCA2_LIM and ORCA4_LIM

ORCA is the generic name given to global ocean configurations using the OPA System. Its specificity lies on the horizontal curvilinear mesh used to overcome the North Pole singularity found for geographical meshes. The common geographical coordinate system has a singular point at the North Pole which cannot be easily treated in a global model without filtering. A solution consists in introducing an appropriate coordinate transformation which shifts the singular point on land (*Madec and Imbard*, 1996; *Murray*, 1996).

Space-time domain

- The horizontal resolution available through the standard configuration is ORCA2. it is based on a 2 degrees Mercator mesh, (*i.e.* variation of meridian scale factor as cosinus of the latitude). In the northern hemisphere the mesh has two poles so that the ratio of anisotropy is nearly one everywhere. The mean grid spacing is about 2/3 of the nominal value. An other resolution (*ORCA4*, with twice less grid point in both horizontal directions) is available. In the *ORCA2* (fig. 2.8) and *ORCA4* configurations the meridional grid spacing is increased near the equator to improve the equatorial dynamics.

- The vertical domain spreads from the surface to a depth of 5000m. There are 31 levels, with 10 levels in the top 100m. The vertical mesh is deduced from a mathematical function of z (Madec and Imbard 1996). The ocean surface corresponds to the w-level $k = 1$, and the ocean bottom to the w-level $k = 31$. The last T-level
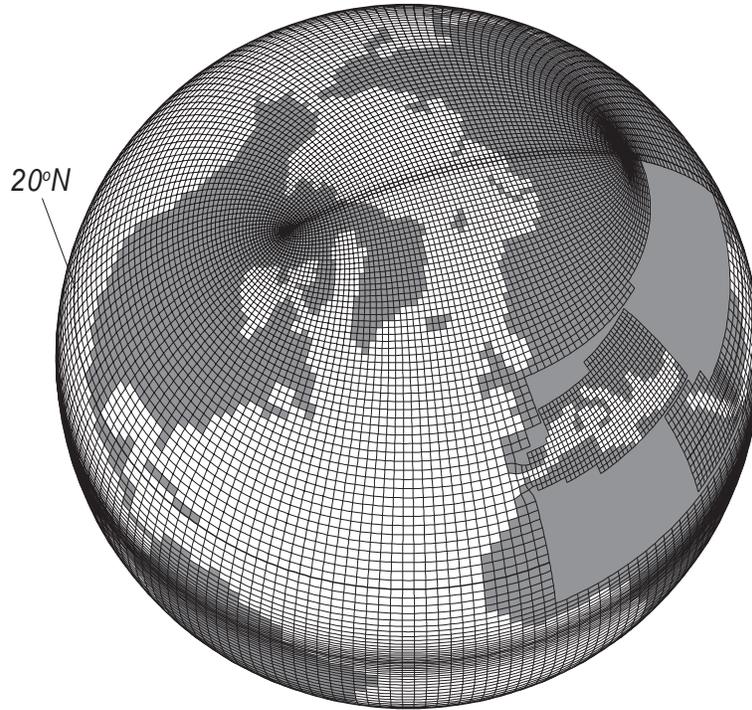
Figure 2.8: Horizontal grid of ORCA 2. The grid is regular (lat-lon) from South Pole to $20°$ North

($k = 31$) is thus always in the ground. The depths of the vertical levels and the associated scale factors is shown in fig. 2.9.

- The time step depends on the resolution. It is $1h36mn$ for ORCA2 so that there is 15 time steps in one day.

Ocean Physics (for ORCA2 LIM in coupled configurations)

- Horizontal diffusion on momentum: the eddy viscosity coefficient depends on the geographical position. It is taken as $40000.m^2/s$, reduced in the equator regions ($2000m^2/s$) excepted near the western boundaries.

- Isopycnal diffusion on tracers: the diffusion acts along the isopycnal surfaces (neutral surface) with a eddy diffusivity coefficient of $2000m^2/s$.

- Eddy induced velocity parametrization with a coefficient that depends on the growth rate of baroclinic instabilities (it usually varies from $15m^2/s$ to $3000m^2/s$).

- Lateral boundary conditions: zero fluxes of heat and salt and no-slip conditions are applied through lateral solid boundaries.

- Bottom boundary condition: zero fluxes of heat and salt are applied through the ocean bottom. The *Beckman* (1998) diffusive bottom boundary layer parameterization is applied along continental slopes. A linear friction is applied on momentum.

- Convection: the vertical eddy viscosity and diffusivity coefficients are increased to $100m^2/s$ in case of static instability.

- Ocean surface: a free surface formulation is used (*Roullet and Madec*, 2000).
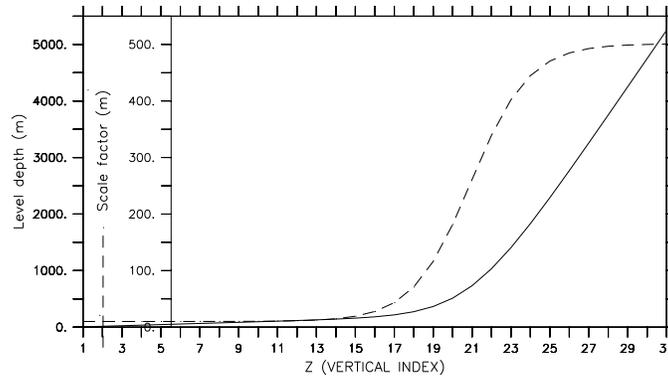
Figure 2.9: Depth of ORCA vertical levels

- Forcings: the ocean receives heat, freshwater, and momentum fluxes from the atmosphere and/or the sea-ice. The sea-ice LIM component is used (see *LIM* documentation). The solar radiation penetrates the top meters of the ocean. The downward irradiance $I(z)$ is formulated with two extinction coefficients (*Paulson and Simpson*, 1977), whose values correspond to a Type I water in Jerlov's classification (*i.e.* the most transparent water).

A reference manual of *OPA* (**?**) is available.

Publications using the *OPA* System can be found on the *NEMO* System web site: http://www.lodyc.jussieu.fr/NEMO. The *OPA* version used in *IPSL_CM4* is described at http://www.lodyc.jussieu.fr/opa.

2.5   The LIM sea-ice model

LIM (Louvain-la-Neuve sea-ice model) is a thermodynamic-dynamic sea ice model specifically designed for climate studies. A brief description of the model is given here. Further details can be found in *Fichefet and Morales Maqueda* (1997, 1999).

Sensible heat storage and vertical heat conduction within snow and ice are determined by a three-layer model (one layer for snow and two layers for ice). The effect of the subgrid-scale snow and ice thickness distributions is accounted for through an effective thermal conductivity, which is computed by assuming that the snow and ice thicknesses are uniformly distributed between zero and twice their mean value over the ice-covered portion of the grid cell. The storage of latent heat inside the ice resulting from the trapping of shortwave radiation by brine pockets is taken into account. The surface albedo is parameterized as a function of the surface temperature and the snow and ice thicknesses. The model also allows for the presence of leads within the ice pack. Vertical and lateral growth/decay rates of the ice are obtained from prognostic energy budgets at both the bottom and surface boundaries of the snow-ice cover and in leads. When the load of snow is large enough to depress the snow-ice interface under the water level, seawater is supposed to infiltrate the entirety of the submerged snow and to freeze there, forming a snow ice cap. For the momentum balance, sea ice is considered as a two-dimensional continuum in dynamical interaction with atmosphere and ocean. The viscous-plastic constitutive law proposed by *Hibler* (1979) is used for computing the internal ice force. The ice strength is taken as a function of the ice thickness and compactness. The physical fields that are advected are the ice concentration, the snow volume per unit area, the ice volume per unit area, the snow enthalpy per unit area, the ice enthalpy per unit area, and the brine reservoir per unit area.

The model equations are solved numerically as an initial value-boundary value problem by using finite difference techniques. A staggered spatial grid of type B is used. The heat diffusion equation for snow and ice is solved by means of a fully implicit numerical scheme, which avoids the development of numerical instabilities when the snow or ice thickness becomes small. The ice momentum balance is treated basically as in *Hibler* (1979), the two main differences being that the oceanic drag term is not linearized and a simultaneous underrelaxation technique is systematically applied. A no-slip condition is imposed on land boundaries. The contribution of advection to the continuity equations is determined by making use of the forward time marching scheme of *Prather* (1986). This method is based on the conservation of the second-order moments of the spatial distribution of the advected quantities within each grid cell. It preserves the positiveness of the transported variables and presents very small diffusion. The interest of employing this elaborate scheme is that for a coarse resolution grid such as the one used here, it allows to determine the location of the ice edge with a higher accuracy than the more conventional upstream schemes do. Worthy of note is that the equations for both ice motion and ice transport are written in curvilinear, orthogonal coordinates, which facilitates the model setup on a large variety of spatial grids. Here, the model runs on the same grid as *ORCA*.

A comprehensive description of the model is avalaible at ftp://ftp.astr.ucl.ac.be/pub/IGL/clio30.pdf.

Chapter 3

The coupled model

3.1 Coupling interfaces

3.1.1 Coupling between atmosphere and subsurfaces

Each atmospheric column has four type of subsurfaces: land, ocean, sea-ice and glacier. The coupling is the same whatever the subsurface model is. For instance, the coupling follows the same method if the SST is readen or is computed by a full oceanic model or by a very simplified ocean (slab ocean). In our approach, the radiative code sees only one surface, with mean properties, and computes only one net flux in both shortwave and longwave domain. Only the turbulent fluxes (sensible, latent, momemtum) are computed separately on each subsurface, and the tendency of the atmopsheric column is the weighted sum of tendencies computed by each subsurface.

The main goals of the new developments are the following:

- to redistribute the radiative fluxes, computed in the atmospheric column, on each subsurface taking into account the local properties of each subsurface;

- to establish a clear interface between the atmopsheric boundary layer code and the surface model, whatever it is.

An absolute requirement is energy and water conservation. In the following paragraphs, subscript i stands for a subsurface i of relative fraction w_i. For each atmospheric column, one has $\sum_i w_i = 1$.

Redistribution of the radiative fluxes

Shortwave flux   The net shortwave flux at surface F^{sw} has been computed by the radiative code for the whole atmospheric columns with an albedo r

$$r = \sum_i w_i r_i \qquad (3.1)$$

where r_i is the albedo of subsurface i. Assuming that the downward shortwave flux is the same above all the subsurfaces, the net shortwave flux F_i^{sw} for each subsurface i may be written as *Dufresne and Grandpeix* (1996):

$$F_i^{sw} = \frac{1 - r_i}{1 - r} F^{sw}. \qquad (3.2)$$

One may verify that energy conservation is ensured (*i.e.* $\sum_i F_i^{sw} = F^{sw}$).

Longwave flux   The net longwave flux at surface F^{lw} has been computed by the radiative code for the whole atmospheric columns with an emissivity ϵ and a temperature T_r

$$\epsilon = \sum_i w_i \epsilon_i \ \ \text{and} \ \ T_r = \sum_i w_i \frac{\epsilon_i}{\epsilon} T_i \qquad (3.3)$$

where ϵ_i is the emissivity of subsurface i and T_i is its temperature. Assuming that the downard longwave flux is the same above all the subsurfaces, the net longwave flux F_i^{lw} for each subsurface i reads *Dufresne and Grandpeix* (1996):

$$F_i^{lw} = \frac{\epsilon_i}{\epsilon} \left(F^{lw} + \frac{\partial F^{lw}}{\partial T_r} (T_i - T_r) \right) \qquad (3.4)$$

with

$$\frac{\partial F^{lw}}{\partial T_r} = 4 \epsilon \sigma T_r^3 \qquad (3.5)$$

30

Interface for coupling the turbulent fluxes

A first standard interface for the coupling between the surface and the atmosphere (*Polcher et al.*, 1998) was proposed by the *PILPS* project. A drawback of the proposed approach is that the separation between the solving of the turbulent fluxes in the boundary layer and the solving of the temperature by the surface model is not complete. Indeed, the time evolution of the first atmospheric level variables (eq. (28) of *Polcher et al.*, 1998)) is a function of the surface flux, but also of some surface coefficients. We overcome this difficulty by rewritting the discretized form of the vertical diffusion equation of the first atmospheric level and by considering explicitly the flux $F_{X,1/2}^{t+\delta t}$ between layer 1 and the surface:

$$\frac{X_1^t - X_1^{t+\delta t}}{\delta t} = \frac{1}{\delta z_1}\left(K_{X,3/2}\frac{X_2^{t+\delta t} - X_1^{t+\delta t}}{\delta z_{3/2}} - F_{X,1/2}^{t+\delta t}\right) \tag{3.6}$$

$$F_{X,1/2}^{t+\delta t} = K_{X,1/2}\frac{X_1^{t+\delta t} - X_0^{t+\delta t}}{\delta z_{1/2}} \tag{3.7}$$

Variables X stands for the dry static energy, the specific humidity or the wind speed; K_X, k is the verical diffusion coefficient for variable X at interface $k-1/2$ (between level k and $k-1$); δz_k is the thickness of layer k and $\delta z_{k-1/2}$ is the distance between the centers of layers k and $k-1$.

In the boundary layer   To solve the vertical diffusion equation in the boundary layer, each variable of level k is written as a function of the variable of the level below $k-1$, for all levels except level 1:

$$X_k^{t+\delta t} = A_{X,k}X_{X,k-1}^{t+Dt} + B_{X,k} \text{ for } k \geq 2 \tag{3.8}$$

For level 1, $X_2^{t+\delta t}$ may be suppressed from eq. 3.6 using eq. 3.8:

$$X_1^{t+\delta t} = A_{X,1}F_{X,1/2}^{t+\delta t} + B_{X,1} \tag{3.9}$$

with

$$A_{X,1} = -\frac{\delta t}{\delta z_1 C_{X,1}} \tag{3.10}$$

$$B_{X,1} = \left(X_1^t + \frac{\delta t K_{X,3/2}}{\delta z_1 \delta z_{3/2}}\right)\frac{1}{C_{X,1}} \tag{3.11}$$

$$C_{X,1} = 1 + \frac{\delta t K_{X,3/2}}{\delta z_1 \delta z_{3/2}}(1 - A_{X,2}) \tag{3.12}$$

One may verify that Eqs 3.9-3.12 make only use of the flux with surface $F_{X,1/2}^{t+\delta t}$ and of atmospheric variables above layer 1. There is no use of surface variable or surface coefficient. For each variable X, variables X_1^t, $A_{X,1}$ and $B_{X,1}$ are transmitted by the boundary layer model to the surface model.

In the surface model   The surface model has to computed the surface flux $F_{X,1/2}^{t+\delta t}$ for each variable X. For the temperature and the humidity at the surface, the new values $X_1^{t+\delta t}$ are computed (if required) through the energy and water budget of the surface. The coupling between atmosphere and surface being implicit, a relationship between $F_{X,1/2}^{t+\delta t}$ and $X_0^{t+\delta t}$ is required. This is obtained by combinig eq. 3.7 and eq. 3.9:

$$F_{X,1/2}^{t+\delta t} = \frac{K_{X,1/2}}{\delta z_{1/2} - K_{X,1/2}A_{X,1}}\left(B_{X,1} - X_0^{t+\delta t}\right) \tag{3.13}$$

31

Net short wave on open ocean
Net short wave on sea ice
Non solar heat flux on open ocean
Non solar heat flux on sea ice
Water budget (precip-evap)
Solid precipitation
 Q/ t (sens+lat) over sea ice
Wind stress over sea ice

LMDZ
Atmosphere

Sea ice fraction
Sea ice albedo (weighted)
Sea ice surface temperature
(weighted)

Wind stress over open ocean
Runoff
Ice sheet melting

LIM
Sea ice

Ocean surface temperature
(weighted)

Net long wave
Non solar heat flux
Stress under sea ice
Fresh water flux
 (concentration/dilution)
Fresh water flux
 (volume flux for free surface)
Sea ice fraction

OPA
Ocean

Ocean surface temperature
Ocean surface salinity
Surface current

Figure 3.1: Coupling fields

3.2 Atmosphere / Ocean / Sea ice coupling

fig. 3.1 shows the fields exchanged between ocean, atmosphere and sea-ice. For most of the fields, the sea-ice model acts as an interface model between atmosphere and ocean. The sea-ice model receive the fluxes for free ocean and sea-ice. It computes the evolution of sea-ice, and then send average fluxes to ocean. Ocean does not know weither its surface is ice covered or not. It receives only mean fluxes. However, the run-off coming from the ocean pours directly into the ocean. The ice calving is considered as a source of pure water for the ocean (see sec. 3.1).

Amongst the fields sent by the atmosphere is dQ/dT. This field is the derivative of turbulent heat fluxes over sea-ice in respect to surface temperature. To compute the temperature at the upper surface of the ice, *LIM* use an implicit scheme with request the derivative of non-solar fluxes. *LIM* computes the derivative of the long wave flux using the 'black corpse' law, and adds the part from turbulent fluxes sended by *LMDZ*.

3.2.1 Time stepping

At the beginning of each coupling time step, the coupler sends the fields to each model. The fields are averaged over a coupling period, generally one day.

In *ORCA*, the fields are received, then sent to the sea-ice model *LIM*, except for the river run-off which is directly send to the ocean. *ORCA* also sends the surface ocean characteristics (sea-surface temperature and salinity, surface currents). The sea-ice model computes the sea-ice evolution and the fluxes (heat, water, salt and momentum). The fluxes are send to *ORCA*. They are identical to thoose coming from the atmosphere for areas free of sea-ice. *LIM* sends also the sea-ice fraction and albedos, which are not needed for the ocean model itself, but are needed for transmission to the atmosphere. *ORCA* then performs a few time-steps (typically 3 or 5) before calling the sea-ice model once again. At the end of the coupling time-step, *ORCA* send the needed fields to the coupler, and wait for its forcing fields fig. 3.2.
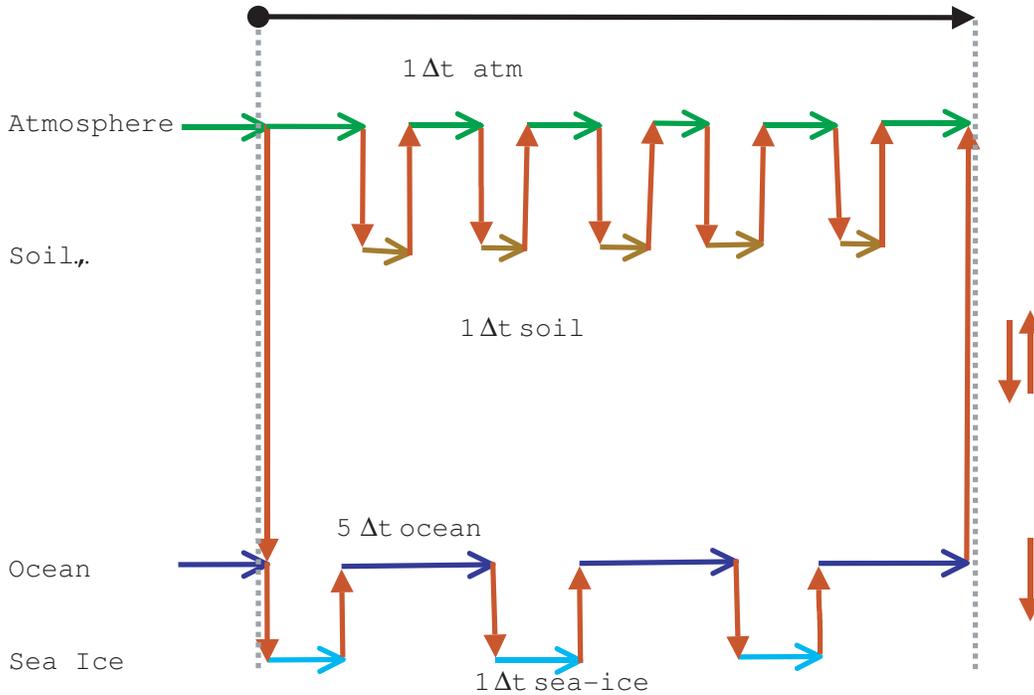
Figure 3.2: Coupling sequence

The fraction of sea-ice is evolving during one coupling time-step. The surface characteristics (temperatures and albedos) sent by the ocean should be coherent with this evolution. For sea-ice albedo for instance, *ORCA* computes the average over the coupling time step $\alpha_{weighted} = \overline{\alpha_{oce.grid} \times fraction_{ice}}^{time}$. In the atmosphere, the model computes the correct albedo with $\alpha = \alpha_{weighted}/fraction_{ice}$. Sea and sea-ice surface temperatures are processed the same way.

At the end of the last time-step of the job, *OASIS* writes all fields in restart files. The following job of the experiment will read these file to initiate the boundary conditions. To start a new experiment, the user should provide these files.

At the ocean-atmosphere interface, the interpolation schemes are designed to conserve extensive quantities globally but also locally. Nevertheless, the time sequence of the model yields to a loss or gain in energy and water. As seen in the figure, the *LMDZ* model compute average surface fluxes over free ocean and over sea-ice during the coupling time step *t-1* (currently one day). These fluxes are then send to *ORCA* which uses them with a sea-ice cover which has evolved, and keeps evolving during the time step *t*. At the end of time-step *t*, the integrated flux received by the ocean could be different, and probably is, from thoose send at the end of time-step *t-1* fig. 3.3.

3.2.2 Snow accumulation

In some regions, the climate could yields to accumulation of snow on grid points, particularly on glaciers. The effect will be a decreased of the sea-level. In the real nature, and if the climate is stable, the dynamics of the ice-sheet should compensate that, through the calving of iceberg. To simulate the calving, the snow mass on a grid point is limited to $3000 kg/m2$. At each time-step, the snow mass over this limit is send to the ocean, after a time-filtering with ten years. The calving benefits a specific interpolation scheme: Earth is divided in three latitude bands with limits at $90°S/50°S/40°N/90°N$. The $40°N$ limits corresponds to the southernmost latitudes reached by iceberg during ice ages (Heinrich events). In each latitude band, the calving is integrated, evenly send to the ocean in the same latitude band. For the northern band, the calving is send to Atlantic and Artic, and not to Pacific.
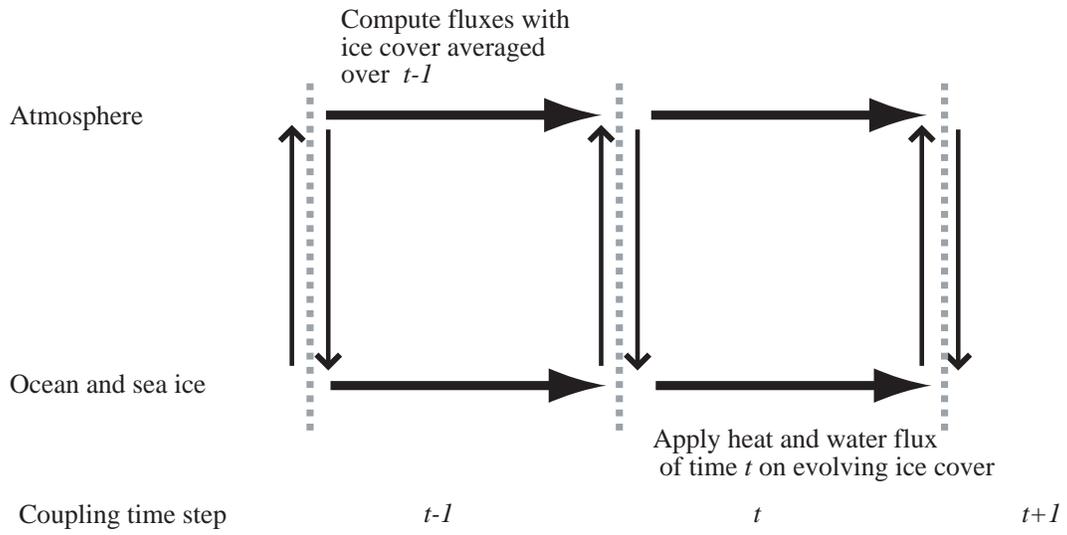
Figure 3.3: Conservation flaw
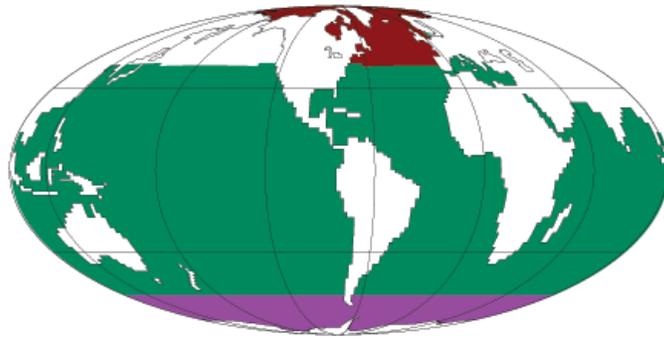
Figure 3.4: The three latitudes bands for 'iceberg calving' melting
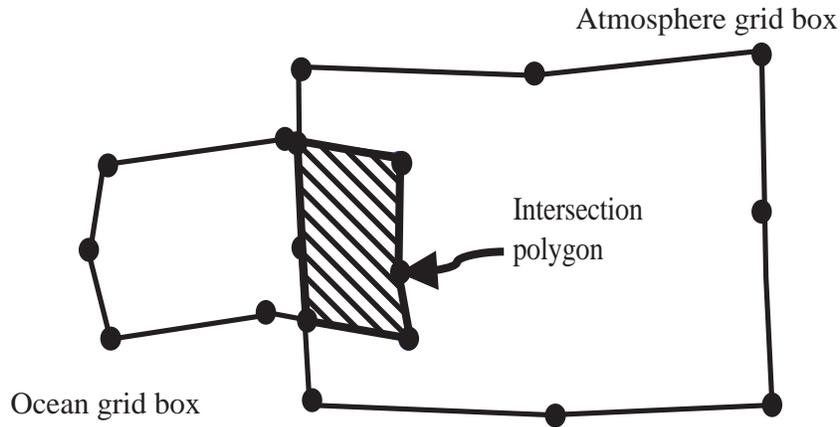
Figure 3.5: The polygon intersection method

3.3 Interpolations

3.3.1 Interpolation of scalars (flux, temperature, ice cover, albedo)

In IPSL CM4 model, the heat and water fluxes, the sea surface temperature, sea ice temperature, and sea ice fraction are interpolated between ocean and atmosphere by *OASIS*, using the interpolation scheme called 'MOZAIC'. *OASIS* does not compute any weight for this scheme. The user should compute the weights outside *OASIS*, and write them in file in the format specified by *OASIS*. This weight computation is the purpose of the software package *MOSAIC*.

The basic of the weight generator is to compute the common surface between any atmosphere grid box with any ocean grid box. With correct normalisation, the ratio bewteen the total surface and the common surface became an interpolation weight. The algorithm used to compute the common intersection between the polygones has been designed and programmed by Jacques Bellier. For mosaic, we have to use the algorithm on the sphere. To do that, we project the coordinates of the polygons on a plane, using a projection with conserves surfaces. The pole of the projection is the center of one of the two polygons.

Usable models

At the begining, around 1996, the *MOSAIC* package was designed to generate interpolation weight between *OPA 7* and *LMD5.3*. *OPA 7* had a northern hemisphere grid with a single pole, and then a simple east-west periodicity condition. *LMD5.3* had a structured grid with a vector point at the poles.

A few months later, the program was adapted for *Arpege* and its Gaussian grid. It was also adapted to *LMDZ* for the *IPSLCM3* of the coupled model.

Then comes the new coupling between *ORCA* and *LMDZ*. For *ORCA*, the only problem was to handle properly the folding condition in the Northern Hemisphere. For *LMDZ*, the grid is unstructured: the Poles are scalar points, and the box around it has 72 sides (with a $72x45$ resolution). This means that this point needs a very specific treatement to have the correct result.

Runoff interpolation

The basics of run-off interpolations are the same than for other water fluxes, except that the interpolation considers only 'coastal' points. Atmosphere point are considered as coastal if there is a fraction of ocean strictly in $]0, 1[$. Ocean points are considered as 'coastal' if they have at least one neighbours being land.
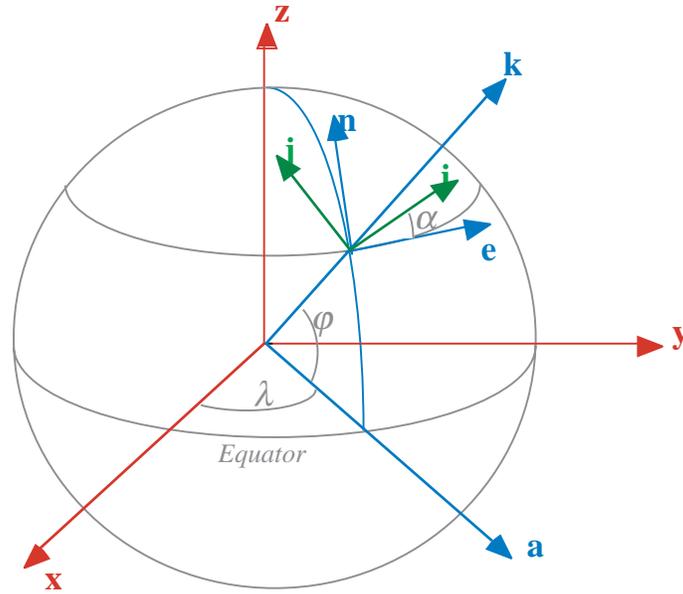
Figure 3.6: The different vectors and referentials used in the wind stress interpolation process. $\vec{e}$ is the unit vector oriented eastward, $\vec{n}$ is the unit vector oriented northward. $\vec{i}$ and $\vec{j}$ are the unit vectors oriented along the ocean gridlines

The river routing paths in *ORCHIDEE* comes from data of water paths. In some time, the difference between the real coast line and the model coastline make it impossible to have the water routed to the ocean. To overcome this problem, the interpolation scheme makes further work. If an atmosphere point is beside a coastal point, its run-off is interpolated to same ocean points lying under this atmosphere points.

3.3.2   Wind stress interpolation

The interpolation of the wind stress, or of any vector field, from the atmosphere to the ocean is a very peculiar problem. The wind stress is defined in a local referential by two components (eastward and northward). Between two grid points, the components are defined in two different local referential. Near the poles, the change of the local referential becomes very large. When we interpolate by doing a weigthed average of 16 components (for a bicubic interpolation), we use 16 different definitions of the local referential. This yields to very strange wind stresses near the poles !!!

To overcome this problem in *IPSL CM4*, we have adopted the method developped at *UCL* to couples *CLIO* and *LMDZ*. We first compute the wind stress components in a unique referential, which is geocentric, linked to the Earth (fig. 3.6). The 3 components are interpolated towards the ocean, and then we compute the local components on the ocean grid. The method give a vertical (normal to the Earth) wind stress component. This component should we 0 when an horizontal vector is interpolated. It is computed in the validation step of the method, which allows to check that it is negligible.

The components are interpolated toward the ocean in the eastward/northward referential. The last step consists to compute the component in the referential of the *ORCA model*. The full method is described in appendix (B.1.1)

The method has been tested in the toy model. The three components was interpolated with a bicubic scheme. In a first attempt, we used the *FSCINT* library enclosed in *OASIS*. But while plotting the vertical component, the problem of periodicity clearly appeared. This shows that computing this component is a good test: the periodicity problem was

not visible while plotting the horizontal components. It was rapidly clear that adapting the *FSCINT* package, an old Fortran 77 (or 66 ?) package comming directly from the 70's, was beyond our courage and intelligence ! We then write from scratch a bicubic interpolator in Fortran 90, which seem more readable and understable. And it works !!!

The wind stress, which in *LMDZ* is a vector defined at the same location that the scalar variables, is interpolated twice: toward the u and v grid of *ORCA*.

Wind stress over the sea ice

LMDZ computes for each grid boxe the wind stress for each kind of surface (land, free ocean, sea ice, glaciers). The wind stress over ocean and sea ice are nealy the same, except when the sea ice fraction is near 0 or 1. Which are the case where the use of fractional grid boxes is supposed to be not very accurate. We decide to use a wind stress which the average of ocean and sea ice stress weighted by the fraction of each surface.

3.3.3 Closed seas

In the ocean model several 'seas' are separated from the global ocean. This is obviously the case of the North American Great Lakes and the Caspian Sea. Due to the limited resolution of the model, seas like the Baltic (low resolution version only) and the Black Sea are also disconnected from the rest of the ocean. The global balance of water is equilibrated in the model: when averaged over the ocean and over several decades, the water flux going into the ocean (net result of precipitation, run-off, calving and evaporation) is zero. But, this is not true for each indivual closed areas : you may have a net transfer of water between the global ocean and the closed seas. To avoid a drift of salinity in both closed seas and global ocean, closed seas benifit a very special treatment. The water budget over each indidual closed sea is set to zero. The water which should pours into each closed sea (or evaporates from) is added to the water budget of the global ocean. We handle the different seas in three differents ways:

- For the Black Sea and the Baltic Sea, the water budget of the closed sea goes to closest oceanic grid point, mimicking the water flux in the straits ;

- For the North American Great Lakes, if the water budget is positive (excess of water), it goes to the ocean, at the mouth of the St-Lawrence river. If it is negative (evaporation), it is spreaded over the whole open ocean ;

- For the Caspian sea, the water budget, either positive or negative, is spreaded over the whole open ocean.

Each closed seas has only a very low number of grid point, which does not allow a relevant resolution of the momemtum equation. Thus the ocean dynamics is degradated : the ocean currents are set to zero, and the diffusion is purely horizontal/vertical (no isopycnal scheme). However, the vertical TKE mixing scheme is fully active.

3.3.4 Future use of OASIS 3

OASIS, in the new version 3, has additional capabilities to interpolate fields, using the *SCRIP 1.4* library (sea http://climate.lanl.gov/Softw The SCRIP library will be tested to replace the MOZAIC interpolation. OASIS 3 has also new features to handled vector fields nicely. This will be tested and hopefully replace the one described here in future version of the IPSL climate model.

3.4   The *OASIS* coupler

OASIS is a coupler, *i.e.* a software interface between different models, written by the *Climate Modelling and Global Change* team at *CERFACS*. It allows the realisation of coupled simulations on different types of platforms, permits the testing of different coupling algorithms (time strategy or interpolation methods for instance), and allow objective inter comparison of coupled GCMs by changing one or both. Quite clearly, the only way to answer these specifications was to create a very modular and flexible tool.

OASIS is a modular and flexible tool, made of a complete, self-consistent and portable set of Fortran 77, Fortran 90 and C routines divided into a main library, interpolation libraries and communication libraries. It can run on any usual target for scientific computing (*IBM RS6000* and *SPs*, *SPARCs*, *SGIs*, *CRAY* series, *Fujitsu VPP* series, *NEC SX* series, etc.). Its main tasks are the synchronisation of the models being coupled, their monitoring, and the treatment and interpolation of the fields exchanged between the models. *OASIS* can couple any number of models and exchange an arbitrary number of fields between these models at possibly different coupling frequencies. All the coupling parameters (models, coupling fields, coupling frequencies, etc.) of the simulation are defined by the user in an input file read at run-time by *OASIS*. The models remain separate entities (different processes in the *Unix* sense). They are unchanged with respect to their own main options (like I/O or multitasking) compared to the uncoupled mode. Few routines need to be added to deal with the time synchronisation and the exchange of coupling fields, realized through *OASIS*. The models can run sequentially or in parallel.

To exchange the coupling fields between the models and the coupler in a synchronised way, four different types of communication are included in *OASIS*. In the *PIPE* technique, named *CRAY* pipes are used for synchronisation of the models and the coupling fields are written and read in simple binary files. In the *CLIM* technique, the synchronisation and the transfer of the coupling data are done by message passing based on *PVM 3.3* or *MPI2*. In particular, this technique allows heterogeneous coupling. In the *SIPC* technique, using *UNIX System V Inter Process Communication possibilities*, the synchronisation is ensured by semaphores and shared memory segments are used to exchange the coupling fields. The *GMEM* technique works similarly as the *SIPC* one but is based on the *NEC* global memory concept.

The fields given by one model to *OASIS* have to be processed and transformed so that they can be read and used directly by the receiving model. These transformations, or analyses, can be different for the different fields. First a pre-processing takes place which deals with rearranging the arrays according to *OASIS* convention, treating possible sea-land mismatch, and correcting the fields with external data if required. Then follows the interpolation of the fields required to go from one model grid to the other model grid. Many interpolation schemes are available: nearest neighbour, bilinear, bicubic, mesh averaging, gaussian. Additional transformations ensuring for example field conservation occur afterwards if required. Finally, the post-processing puts the fields into the receiving model format.

3.5   Model environment

3.5.1   MODIPSL

MODIPSL is a tool developed (in *Korn Shell* and *Python*) by *IPSL* modelling pole engineers with the aim of providing a common access and a common interface to each of the *IPSL* different models. *MODIPSL* is structured around two main building blocks that propose:

- A working environment common to the different models and which can be deployed on any type of platform;

- A set of standard commands facilitating the use and functioning of the models. This set of commands is based on the following principles:

    - Mutualisation of the access to the different models' sources;
    - Adaptation of these commands, to a given platform, in order to generate the appropriate executable files.

The common environment takes form through a uniformed directory structure nonetheless respecting the specific characteristics of each model, from the coupled model *IPSLCM4_v1* (LMDZOR, ORCA, LIM and ORCHIDEE). Note that prior to using the commands on a given platform, the functional validation of a model, on this platform, is required. Currently, installation and functioning of the coupled model have been validated on the *NEC SX5* at *IDRIS*, on the *Fujistu VPP5000* and *NEC SX6* at *CEA* and on the *Eart Simulator* at Yokohama. Considering the above framework, *MODIPSL* enables the extraction, installation, compilation and execution of any model but also the analysis of its output data.

Prior to using the *MODIPSL* functionalities the following installations are required:

- *CVS* software;

- *NetCDF* library compiled ;

- *Fortran 90* compiler;

- *Python* software;

- The *CDAT* library of Python;

- *Ferret* software;

- *NCO* and *NetCDF* operators.

MODIPSL must be extracted from a *CVS* server and then installed on the given platform. This fitting provides the necessary tools for the extraction and installation of the desired model.

Note that the `mod.def` file contains the description of all the information concerning each *IPSL* model. Note also that the `model` command extracts (from one or several *CVS* servers) then installs the model components which name has been passed on argument. In addition, texttmodel offers some maintenance functions for the installed models.

Once the installation is finished, compiling requires the use of the `ins_make` command. It enables the installation and configuration of the models makefile based on the working platform. Before executing the model, the final step consists in configuring the desired simulation. This is done by editing physical parameterisation and launching files:

- Activating or not physical parameterisation;

- Specifying time limits and simulation memory needs;

- Defining start time, end time and output frequency;

- Activating or not post-treatment flags.

Installing the submission job of the fully parameterized simulation requires using `ins_script` command. This command can also be used to configure the job depending on the simulation platform as well as attribute a name to the simulation. The following command series illustrates the above-defined steps as well as the simulation configuration. The example is given for the platforms *Rhodes* (*SGI2100*) and *Uqbar* (*NEC SX5*). It is also possible to compile on a station and to launch the simulation on another calculator. Note also that in order to launch a simulation, the access to input files stored on *IDRIS* or *CEA* file servers, or a *DODS/OPeNDAP* server is mandatory.

The output files are stored on the files servers (*Gaya* for the *IDRIS*, *Cosmos* for the *CEA/CGCV*, and *Fer* for *CEA/CCRT*) in identical directory trees for each model component. These results can be compared to *IPSL* reference simulation results.

A full description of *modipsl* is available at http://www.ipsl.jussieu.fr/~ioipsl/IPSLCM4/index.html, including a quick starting guide and a full launching guide for *IPSLCM4_v1*.

3.5.2 Graphics and automatic post-processing

Post-processing on NetCDF[1] models output files have been made using NCO[2] operators. This concerns modifications and corrections of variable attributes stored in NetCDF model output files in order to respect the Climate and Forecast convention but also creation of decade seasonnal output. More informations on this convention can be found at http://www.cgd.ucar.edu/cms/eaton/cf-metadata.

If post-treatment flag is activated, a collection of *NetCDF* time-series files are created during the simulation. From those *NetCDF* files, a monitoring is processed and results images are put on the selected *OPeNDAP* server to let the user follows and controls his simulation. The monitoring based on Ferret[3] and the *FAST-ATLAS* framework consists in the realisation of time plots, latitude/time plots and spatial maps. Those monitored key-variables have been carefully selected to help the user in the decision to continue or to stop the simulation.

In addition to the monitoring, dedicated diagnostics for each component of the *IPSL* coupled model are proposed to the user along the simulation every 10 years using decade seasonnal output produced by the post-precessing part. This graphics processing based on Ferret and the *FAST*-ATLAS framework proposes to the user selected diagnostics, mainly spatial maps and zonal averages, for a selected variables of each components: atmosphere, ocean, sea ice, vegetation, runoff, marine biochemical models. Some diagnostics produce comparisons between the model output and a referenced quality and updated data (satellite products, simulation control model output). Others propose atmospheric fields at standard level pressures or sea ice model maps centered on poles.

FAST-ATLAS is a collection of *Ferret* scripts and `Ksh` scripts designed to facilitate layout and creation of diagnotics. A description of this framework is available at http://dods.ipsl.jussieu.fr/fast including installation procedures, tutorials and usage examples made during *IPCC* runs.

---

[1] http://www.unidata.ucar.edu/packages/netcdf
[2] http://nco.sourceforge.net
[3] http://www.ferret.noaa.gov

Chapter 4

Model climatology

We present below some aspects of the simulated mean climatology and variability, and compare results obtained with two versions of the model (table 4.1) and two model resolutions, LMDZ 96x71x19 / ORCA2 and LMDZ 72x45x19 / ORCA4. This allows to show robust characteristics of the model, and the impact of recent adjustments. Part of the simulated climatology is a compromise between subtle adjustments, which are limited by the fact that regional features need to be properly represented using parameterizations that need to be valid for the entire globe. The aspects shown here are representative of the reference versions described below. They may vary slightly depending on the length of the simulation, and small additional model adjustments. More complete atlases of the different simulations can be found on the "Pôle de modélisation" web site[1]. In this document we only consider long term tendencies and mean annual cycles. Ongoing analyses on climate variability suggest interesting behaviour of the model but are note reported here.

4.1 Differences between the two model versions

The version we consider as reference corresponds to the summer 2004 release of the model. This version was use to run the IPPC and CMIP simulations. It includes a control simulation (2L20[2]) with concentration of the different trace gazes prescribed to modern trace gazes concentration, a pre-industrial simulation (2L24[3]) with trace gazes concentration prescribed to pre-industrial values (circa 1750), a CMIP simulation (2L23[4]) with 1% increase in the CO_2 concentration until quadrupling CO_2 is reached, and two additional stabilization scenarios with respectively $2xCO_2$ (2L23B[5]) and $4xCO_2$ (2L2C3[6]) starting from the *CMIP* run when the corresponding level of CO_2 is reached. The full set of IPCC simulations performed at IPSL are described at http://mc2.ipsl.jussieu.fr/simules.html.

We also consider two earlier simulations made with the model released in 2003: LJ7[7], and BR01, a simulation at lower resolution (LMDZ 72x45x19 / ORCA4). Several modifications have been made compared between the 2003 and 2004 versions (table 4.1). They concern:

- the treatment of the phenology of vegetation ;

- the adjustment of the atmospheric boundary layer under stable conditions in order to improve the shape of the atmospheric inversion in subsiding regions and to correct a warm bias over the Eurasia and Siberia during winter;

---

[1] http://www.ipsl.jussieu.fr
[2] http://dods.ipsl.jussieu.fr/mc2ipsl/2L20/2L20.php
[3] http://dods.ipsl.jussieu.fr/mc2ipsl/2L24/2L24.php
[4] http://dods.ipsl.jussieu.fr/mc2ipsl/2L23/2L23.php
[5] http://dods.ipsl.jussieu.fr/mc2ipsl/2L23B/2L23B.php
[6] http://dods.ipsl.jussieu.fr/mc2ipsl/2L23C/2L23C.php
[7] http://dods.ipsl.jussieu.fr/mc2ipsl/LJ7/LJ7.php

Model version	summer 2003	IPCC version
Name	LJ7 (ORCA2 / LMD 96x71) and BR01 (ORCA4 / LMD 72x45)	2L20 (ORCA2 / LMD 96x71)
Averaging period used to compute the mean seasonal cycle	1909-1958 (LJ7) and 51-120 (BR01)	1851-1940 (2L20)
Full atlases	http://dods.ipsl.jussieu.fr/mc2ipsl/LJ7/LJ7.php	http://dods.ipsl.jussieu.fr/mc2ipsl/2L20/2L20.php

Table 4.1: Table of simulations shown in this chapter

- several adjustments over sea-ice to prevent the tendency of too large sea-ice growth;

- the tuning of the ocean albedo, which is used to balance the radiative fluxes of the model in a way that counteract the fact that in this model version the radiative forcing of aerosols in not considered. Additional online diagnostics have also been implemented to meet international project standards;

- correct a bug on the melting of snow over sea-ice.

Several studies have been made with this model, with both model versions, including a set of paleoclimate simulations for the mid-Holocene and the last glacial maximum in the frame of the MOTIF[8] European Project and PMIP II[9] international project. The sensivity to fresh water fluxes has been performed by *Swingedouw et al.*

Only control simulations will be considered in the following, since they are the only simulations that can be compared to modern climatology.

All simulations are started with the same procedure. The ocean starts from rest with temperature and salinity set to the values of the *Levitus* (1982) atlas. The sea-ice characteristics correspond to a ten years adjustment of the sea-ice model from a forced ocean-ice simulation. The atmosphere is initialized from the *ECMWF* (*ERA15*) for 1979, January1st. The land surface model starts with soil moisture initialized to 300 mm at each grid point. At the beginning of the simulation, the model builds its vegetation cover, and the routing scheme at the resolution of the atmospheric model. Over all the surfaces the snow reservoir start from zero. With this procedure, the first ten years of the simulation correspond to rapid adjustments between all the models. They are not representative of the longer time scale evolution of the simulation. The major surface characteristics do not vary much after 30 years.

For this note, the mean seasonal cycles were computed from year 1850 to 1940 of the 2L20 simulation, from year 51 to 120 for BR01, and from year 1909 to 1958 for LJ7.

4.2 General overview of model results

An important aspect of the model development was the closure of the energy and water budgets. This requires that the net budget at the top of the atmosphere is zero, so that the system doesn't store or loose energy when integrated for several years or centuries. To reach this goal without spurious departure from modern climatology this requires that the net heat flux at the top of the atmosphere in forced sea-surface temperature (observed) simulation with the atmospheric model is nearly zero when averaged over the globe and over a few years. With this criterion, the global drift of the coupled model is limited. However, it doesn't prevent drifts in the surface temperature that may arise from changes in the ocean heat storage or from long-term drift in the snow cover, sea-ice or any of the reservoirs with long time constants.

In the reference version (2L20), the net heat flux is closer to zero than in LJ7 and BR01 (fig. 4.1), and the model adjusts more rapidly, with a sligthly lower global temperature (fig. 4.2). However, tendency of surface temperature

---

[8]http://www-lsce.cea.fr/motif

[9]http://www-lsce.cea.fr/pmip2
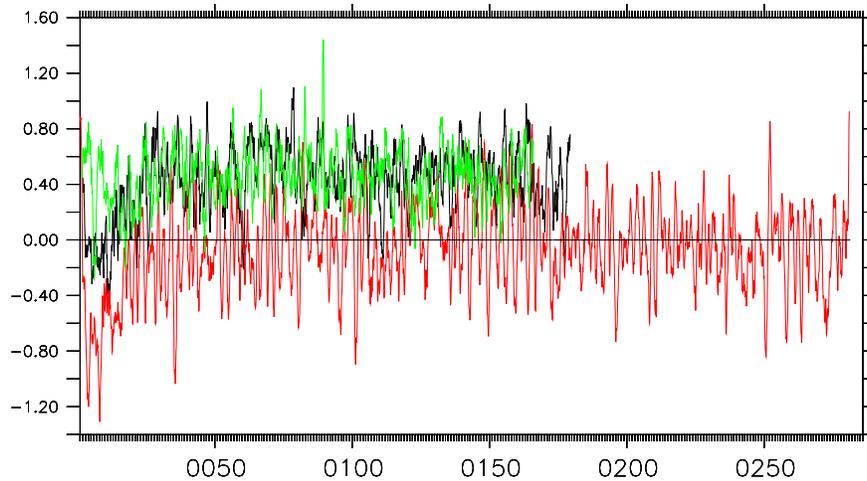
Figure 4.1: Heat flux budget at the surface (W/m^2), globaly averaged and boxed smoothed over 12 months. Black: LJ7, red: 2L20 and green: BR01. Time axis in year.

reflect also local internal feedbacks that occurs mainly where subsidence is large and over see-ice and the sea-ice margin.

Heat flux adjustment   In coupled mode, the net heat gain at the surface during the first years of coupled simulations reflects the imbalance between the initial state of the different models (fig. 4.1). This unbalance is absorbed in about 5 to 20 years in the model.

In LJ7 and BR01, the net flux remains positive, and the ocean heat content slowly drifts. In 2L20, further adjustments of the model allows a net flux very close to zero. The largest difference between LJ7 and 2L20 is dominated by changes in the boundary layer over the continents, changes in the sea-ice and the reduction of the ocean albedo.

Evolution of temperature and salinity   The evolution of sea surface temperature (SST, fig. 4.2) is consistent with the net heat flux, with a cooling during a few decades when surface loses energy, and a stabilization. After 50 years of simulation the mean surface pattern does not evolve much. The differences of temperatures between the simulations reflect the differences in surface fluxes. The rapid ajustment of the surface ocean should not mask that deeper layer are not in equilibrium and still adjusting from the initial state.

LJ7 and 2L20 have very similar evolution of temperature in the upper layer 0-100m. Going further deep, 2L20 is much stable, with a global drift of circa $0.07°C/century$ for 2L20. LJ7 has a global drift twice larger or more at all depths below 1000m.

The change between LJ7 and 2L20 show a very large impact on salinity at all depth. The main effect is probably the closure of the water budget on glaciers in 2L20. In 2L20, salinity is very stable from surface to 1000m. The drift is less than 0.03 $PSU/century$ in between 1000 and 2000m, and less than 0.01 $PSU/century$ below.

Sea surface temperature   The mean features of the the SST pattern are the very close for the three simulations (fig. 4.5, fig. 4.6 and fig. 4.7). The ocean is too warm in the eastern tropics, whereas western basins are correctly simulated. The equatorial upwelling is located to far west in the tropical Pacific. This feature is associated to too strong trade winds in the middle of the basin. Fig. 4.6 shows that the SST difference between the 2L20 simulation and climatology doesn't exceed 1°C in most of the tropical regions. Similar tendencies can be found in the equatorial Atlantic ocean. The equatorial upwelling is located in the middle of the basin does not extend from the African coast, and the gulf of Guinea has a warm bias. From the different adjustments made to improve the model climatology,
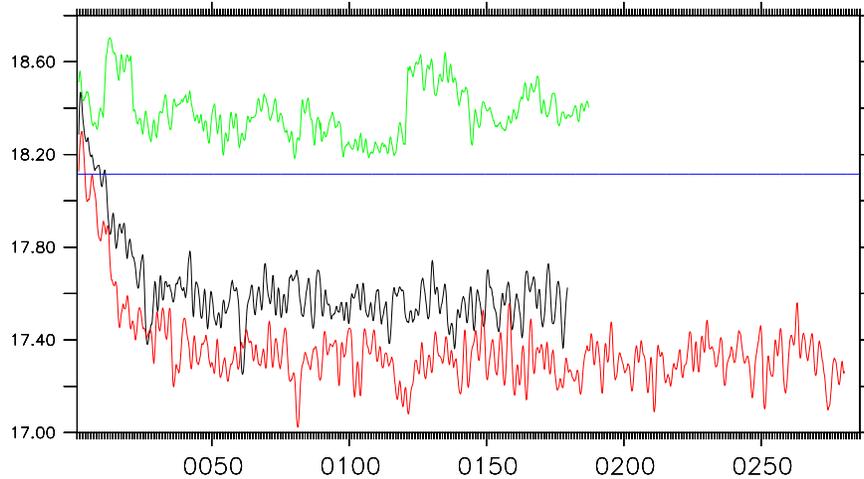
Figure 4.2: Sea surface temperature, globaly averaged and box smoothed over 12 months (Celsius). Black: LJ7, red: 2L20 and green: BR01. Blue line is observation from HadSST. Time axis in years.

we know that the magnitude of these features is sensitive to small radiative adjustments. The main bias is the cold mid-latitudes in all basins. In middle and high latitude the model present a cold bias that can be related to a shift of the atmospheric structures (winds) towards the equator and to a too large extent of sea-ice in the Arctic.

The major difference north of $50°$N between LJ7 and 2L20 is the reduction of the warm bias in North Pacific and a slight cooling in North Atlantic. This may be due to colder conditions over land in 2L20. Note that the tropical SST are not affected by the changes. The low resolution version produces patterns similar to BR01, but magnitude of biases are larger, with a large heating at southern high latitudes.

Precipitation The coupled model simulations (fig. 4.8) reproduce some of the good characteristics of the precipitation distribution found in atmosphere alone simulations with the Emanuel convection scheme and the new formulation of clouds (see section 2.2.3). They concern: The relative magnitude of precipitation between land and ocean in the southern hemisphere in winter, the position and the seasonal march of the ITCZ over the ocean, precipitation in the Indian ocean, and the relative intensity of precipitation between the warm pool and the South Pacific Convergence Zone (SPCZ). However the model also have some common biased such as the tendency to produce a too strong double ITCZ structure in winter, and the too zonal distribution of precipitation in the SPCZ. The intensity of the double ITCZ is somewhat sensitive to model resolution. The model produces also too much precipitation in middle latitudes, which is a feature already found in atmosphere-alone simulations, and does not appear in the low resolution version. These excess precipitations has been identify as a cause of freshening of the Artic.

Sea-ice Sea-ice cover ajusts with the a time scale similar to SST (fig. 4.9 and fig. 4.10). The sea-ice cover simulated by LJ7 is slightly underestimated in northern hemisphere, where 2L20 does a very good job compared to the observations of *Gloersen and Campbell* (1991) (fig. 4.11, fig. 4.13 and fig. 4.12) . The adjustment of the atmospheric model are such that the simulated climate in 2L20 is colder by about $4°$C in high latitudes, which favors the build up and extend of sea-ice. The large scale pattern of simulated ice cover is in qualitative agreement with climatology and the timing of the seasonal cycle is correctly phased (fig. 4.9 to fig. 4.14). The Labrador sea is covered by ice, whereas the ice extension in the northwest Pacific is not fully developped. In the southern hemisphere, the seasonal cycle is overestimated and sea ice almost vanishes in summer. The low resolution simulation BR01 does not correctly the sea-ice margin in the Arctic. The region where sea-ice patterns show the largest differences between simulations corresponds to the largest differences in sea surface temperature near the sea ice margin over the Arctic.
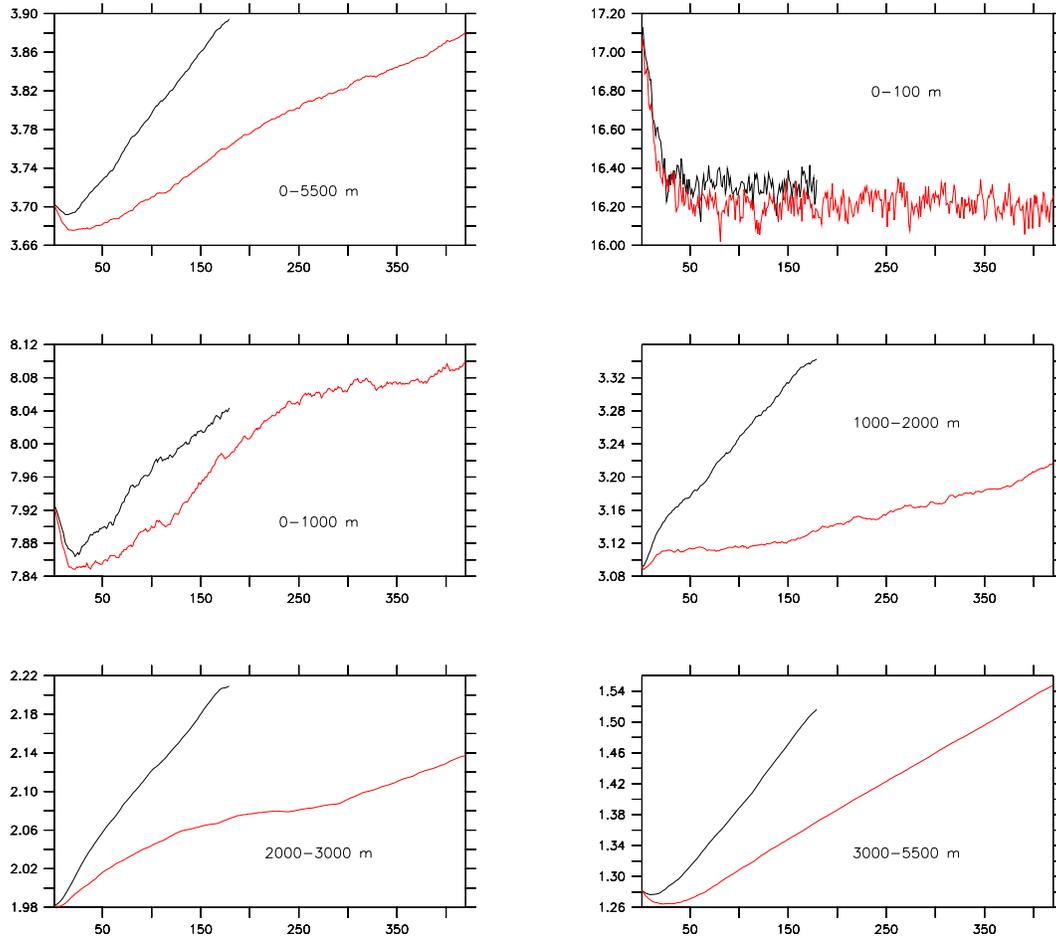
Figure 4.3: Evolution of oceanic temperature (Celsius), yearly averages, for LJ7 (black) and 2L20 (red). Time axis in year. From left to right and top to bottom: 1) global temperature, 2) upper layer (0-100m), 3) 0-1000m, 4) 1000-2000m, 5) 2000-3000m and 6) bottom layer (3000-bottom).
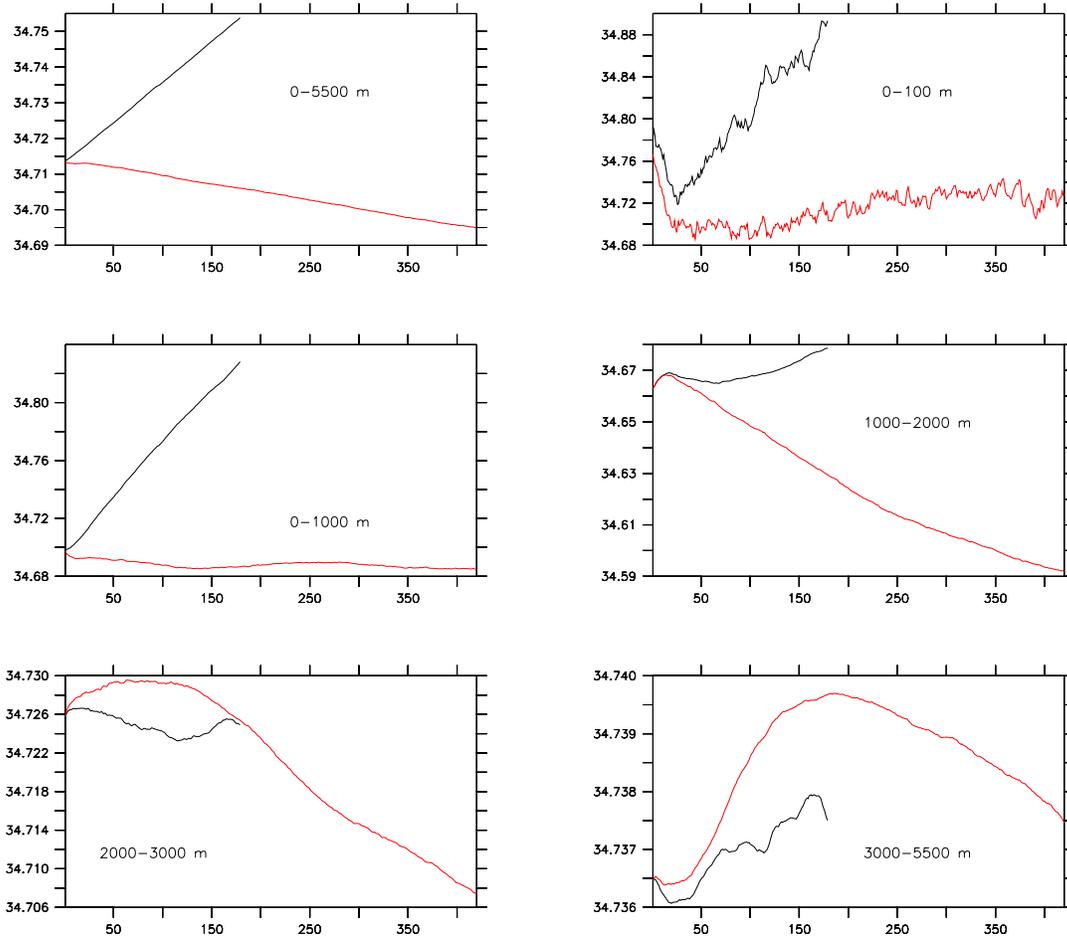
Figure 4.4: Evolution of oceanic salinity (PSU), yearly averages, for LJ7 (black) and 2L20 (red). Time axis in year. From left to right and top to bottom: 1) global temperature, 2) upper layer (0-100m), 3) 0-1000m, 4) 1000-2000m, 5) 2000-3000m and 6) bottom layer (3000-bottom).
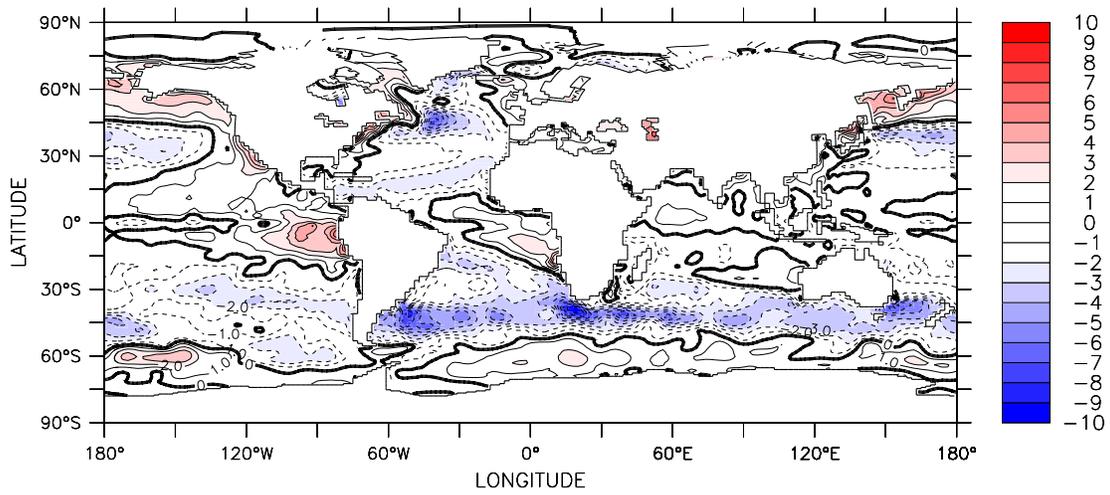
Figure 4.5: Sea surface temperature. Difference between LJ7 and *Levitus* (1982) data. Contour interval 1°C.
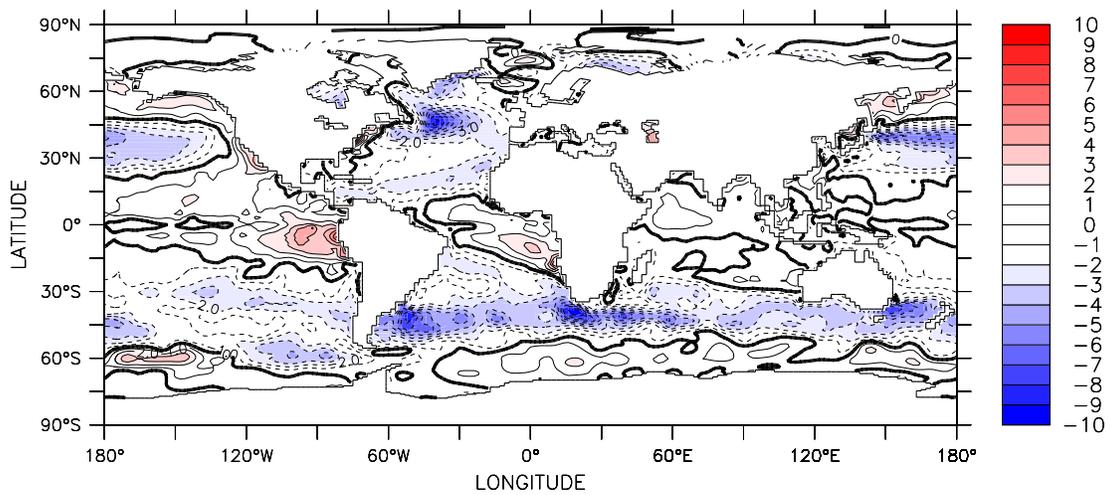
Figure 4.6: Sea surface temperature. Difference between 2L20 and *Levitus* (1982) data. Contour interval 1°C.

47
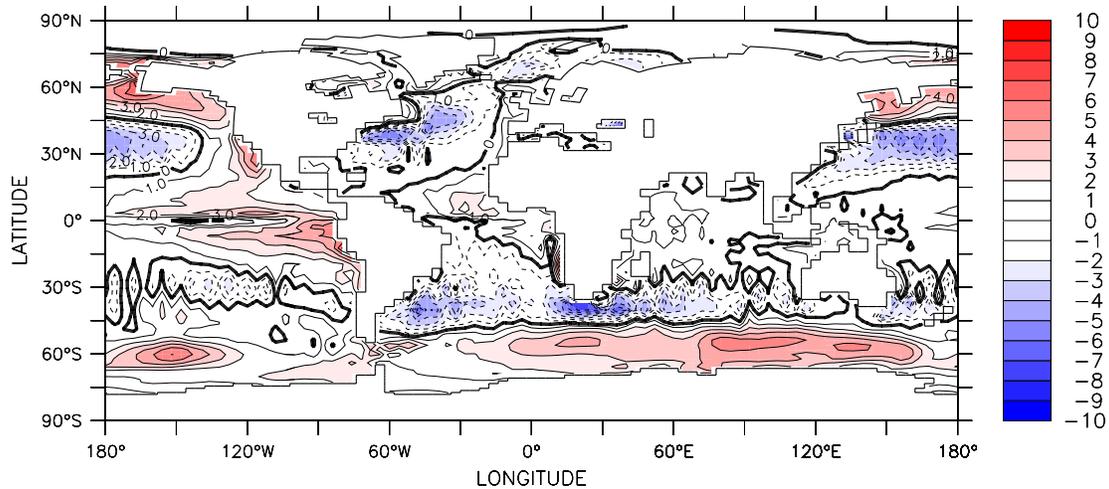
Figure 4.7: Sea surface temperature. Difference between and BR01 and *Levitus* (1982) data. Contour interval $1°$C.

Surface salinity Surface salinity integrates the effects of the different fresh water sources and sink, precipitation, evaporation, river runoff, ice calving, sea-ice. SST and precipitation can be in part related to the structure and magnitude of the different surface fluxes. These fields are difficult to compare to climatology, since these climatology large errors, depending on the regions. The range of surface salinity simulated by the model is comparable with *Levitus* (1982) data. The model does not fully maintain the salinity contrast between the Atlantic and other oceans. Low saline water invade the sea-ice margin and the north Atlantic. Shift in monsoon rain leads to too fresh waters in the region of the maritime continent and too salty waters in the bay of Bengal. The lack of precipitation over the Amazone drainage basin translate also to too saline waters at its mouth in the Atlantic ocean. The advection of salty water from the subtropical Atlantic is insufficient to maintain the thermohaline circulation (*Swingedouw et al.*).

Zonal average of temperature Figure 4.17 shows the zonal mean of temperature for ocean and atmosphere. The model presents a cold bias in atmosphere except in the tropics. The maximum cooling is located at 200-300 hPa. This cold bias also translates into ocean, where the bias is less than 2$°$C in most locations.

Temperatures at the equator The vertical slice of temperature at the equator (fig. 4.18) mainly reflects the wind regime in the region, together with the quality of the ocean vertical scheme (e.g. *Blanke and Delecluse*, 1993). LJ7 and 2L20 succeed to maintain the vertical and zonal temperature gradient close to observation. In BR01 the larger lateral viscosity needed to prevent numerical noise diffusion affects the equatorial currents and thermal structure (*Maes et al.*, 1997). The model also succeeds to maintain the east-west gradient in the Atlantic, even with the low resolution model. This feature was very badly simulated in the *IPSLCM1* model. Note that the reference version (2L20 experiment) is slightly warmer than the earlier version. The warm bias in the Gulf of Guinea is more pronounced.

4.3   Key features of the tropical circulation

Even though the model is not perfect, several features are well reproduced in particular in the tropical regions. They concern the radiative adjustment of the model and the seasonal phasing of the mean seasonal cycle. This enhances our confidence in using this model for future climate change scenarios that can be considered as radiative perturbations of the climate system and for studying some aspects of climate variability and changes in climate variability. We will highlight thes features below.
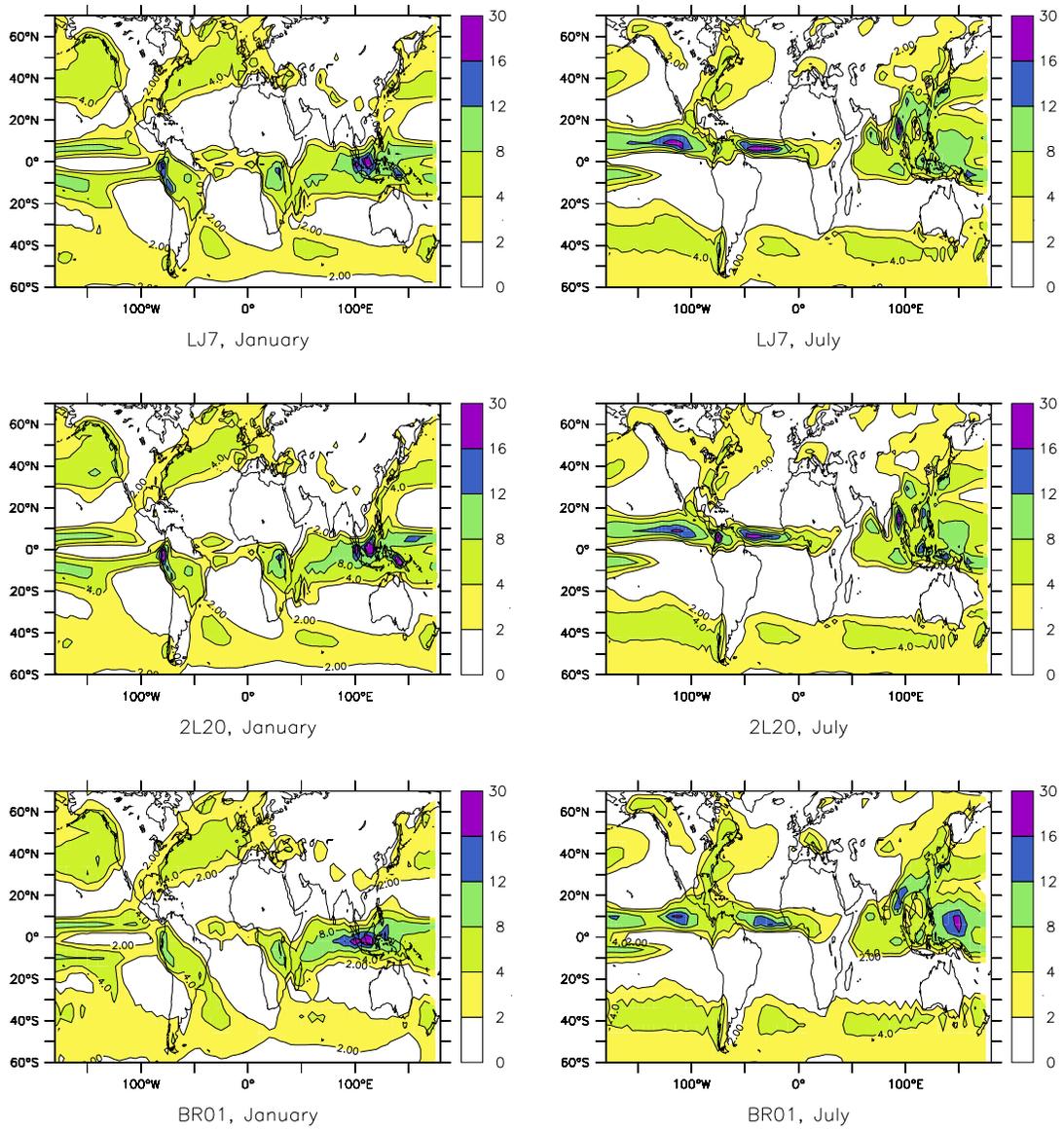
Figure 4.8: Precipitation. Left column is January, right column is July. Top: LJ7, middle: 2L20, bottom: BR01. Contour interval at 2, 4, 8, 12, 16 and 30 mm/day. Observed precipitation are shown in fig. 2.1 an fig. 2.2
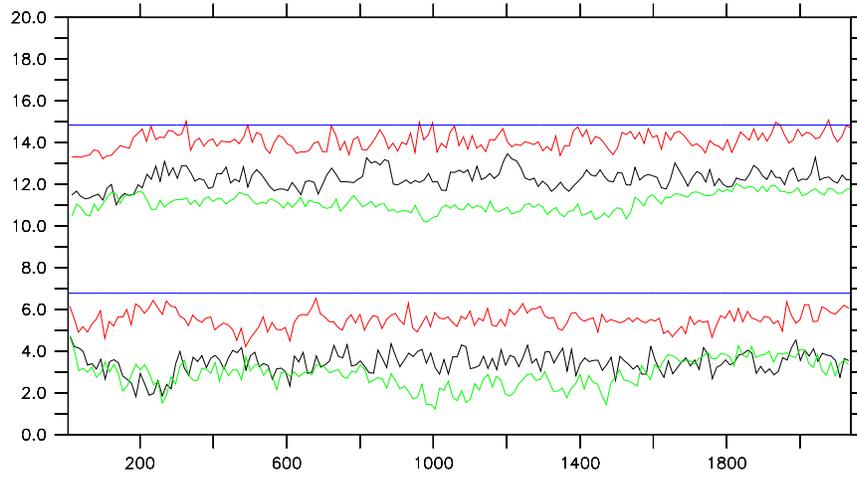
Figure 4.9: Sea ice surface : yearly maxima and minima for northern hemisphere in $10^6 km^2$. Black: LJ7, red: 2L20 and green: BR01. Blue lines are observations (*Gloersen and Campbell*, 1991). Time axis in month.
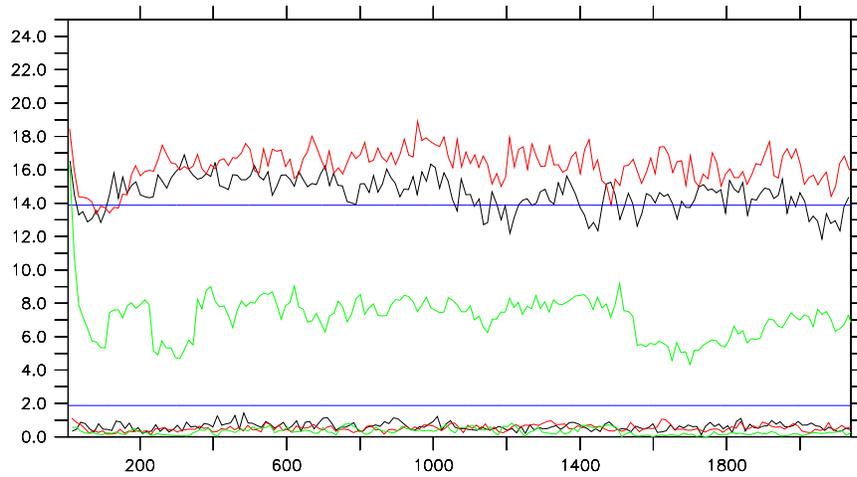

Figure 4.10: Sea ice surface : yearly maxima and minima for southern hemisphere in $10^6 km^2$. Black: LJ7, red: 2L20 and green: BR01. Blue lines are observations (*Gloersen and Campbell*, 1991). Time axis in month.
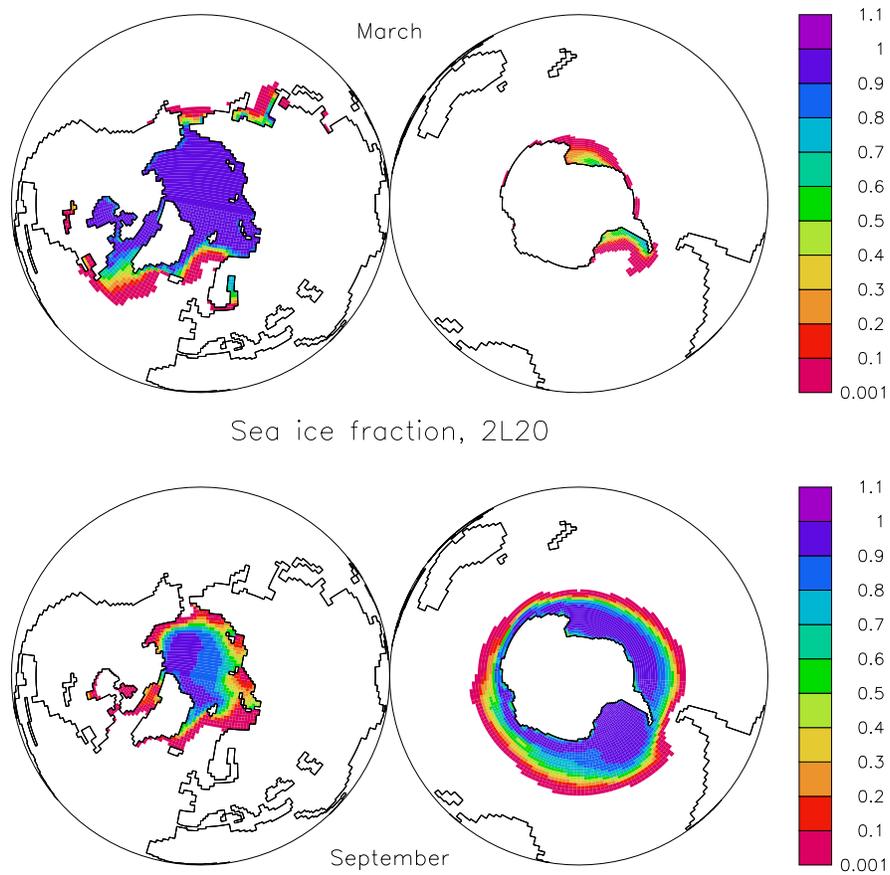
Figure 4.11: Sea ice cover (fraction), 2L20. Top: March, bottom: September. Contour interval is 0.1.

March

Sea ice fraction, Observations
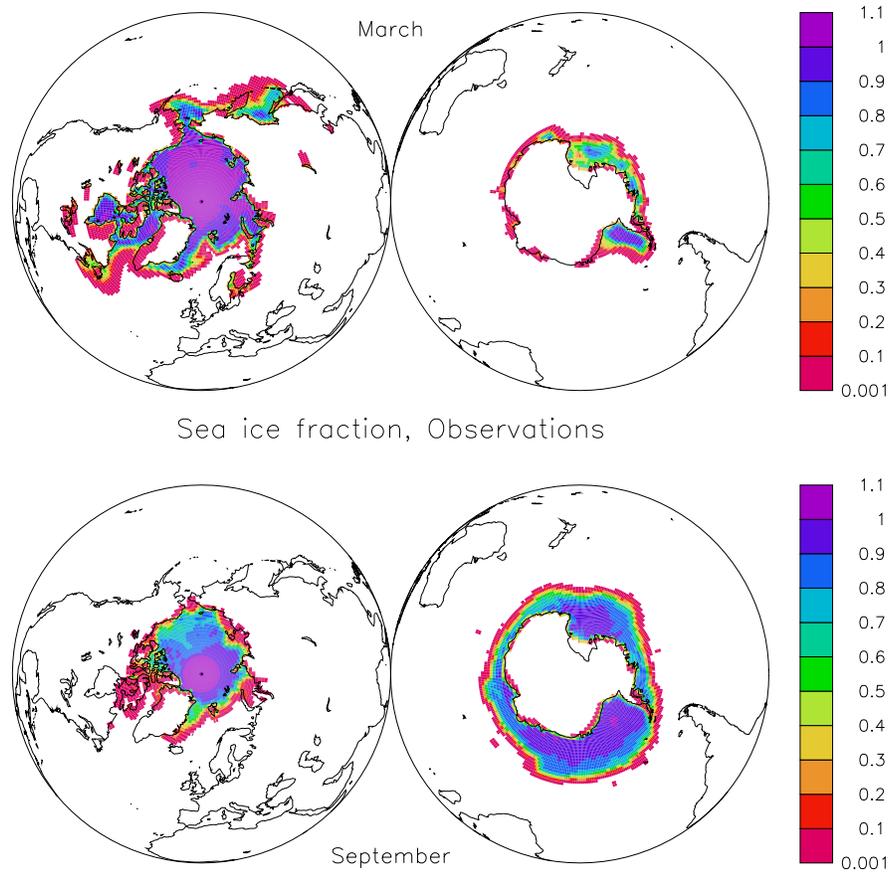
September

Figure 4.12: Sea ice cover (fraction), observations (*Gloersen and Campbell*, 1991). Top: March, bottom: September. Contour interval is 0.1.
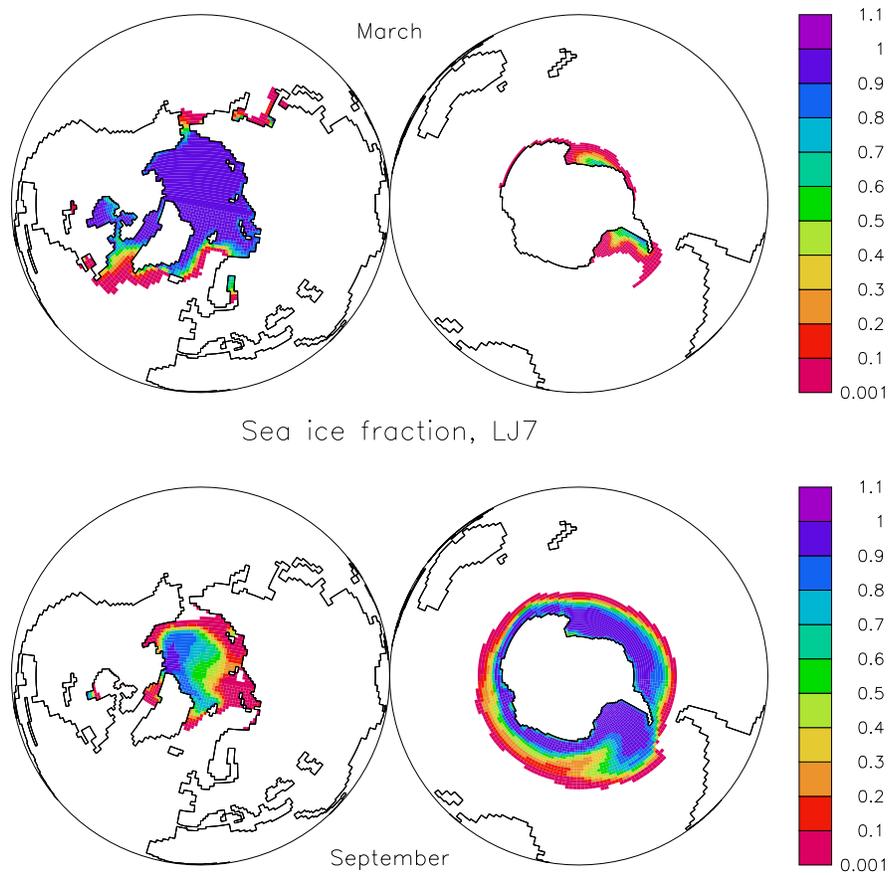
Figure 4.13: Sea ice cover (fraction), LJ7. Top: March, bottom: September. Contour interval is 0.1.
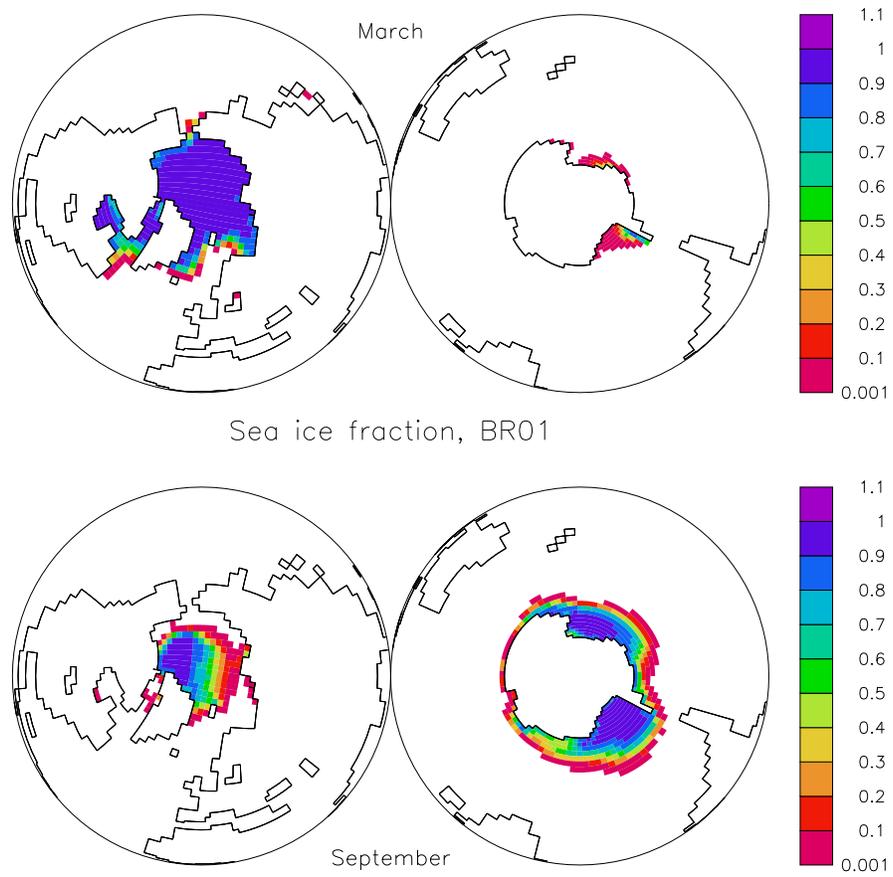
Figure 4.14: Sea ice cover (fraction), BR01. Top: March, bottom: September. Contour interval is 0.1.
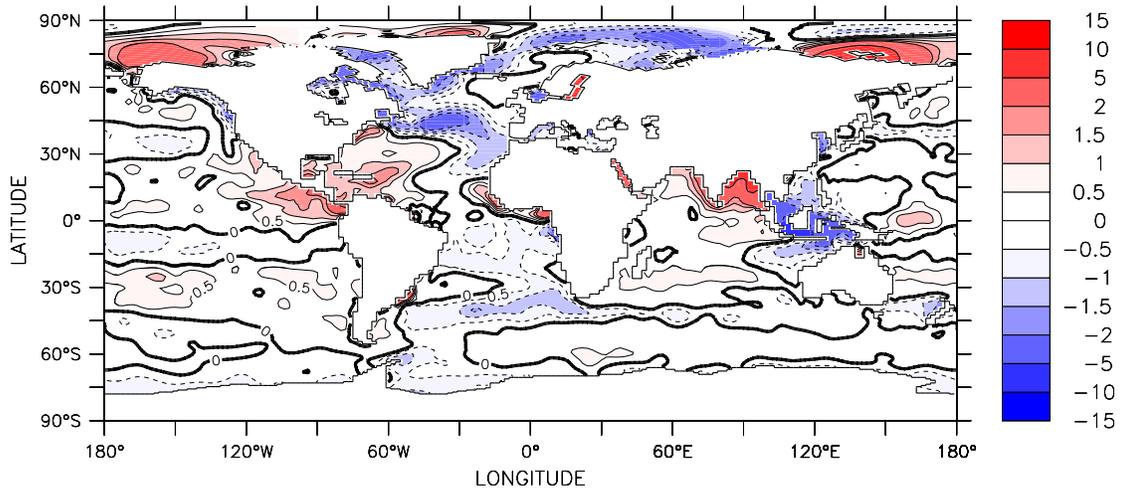
Figure 4.15: Sea surface salinity. Difference between LJ7 and *Levitus* (1982) data. Contour interval 0, ±0.5, ±1, ±1.5, ±2, ±5, ±10 and ±15 PSU.
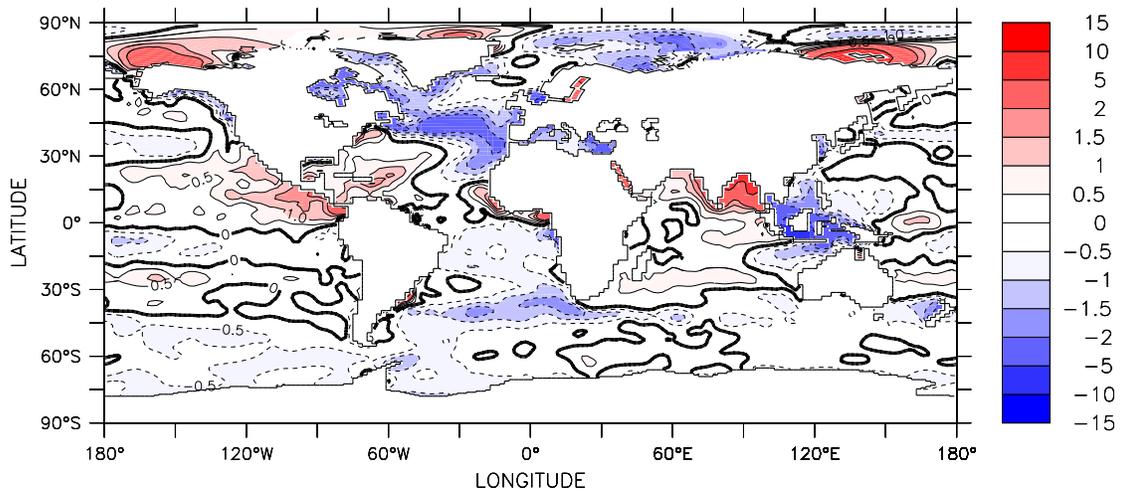
Figure 4.16: Sea surface salinity. Difference between 2L20 and *Levitus* (1982) data. Contour interval 0, ±0.5, ±1, ±1.5, ±2, ±5, ±10 and ±15 PSU.
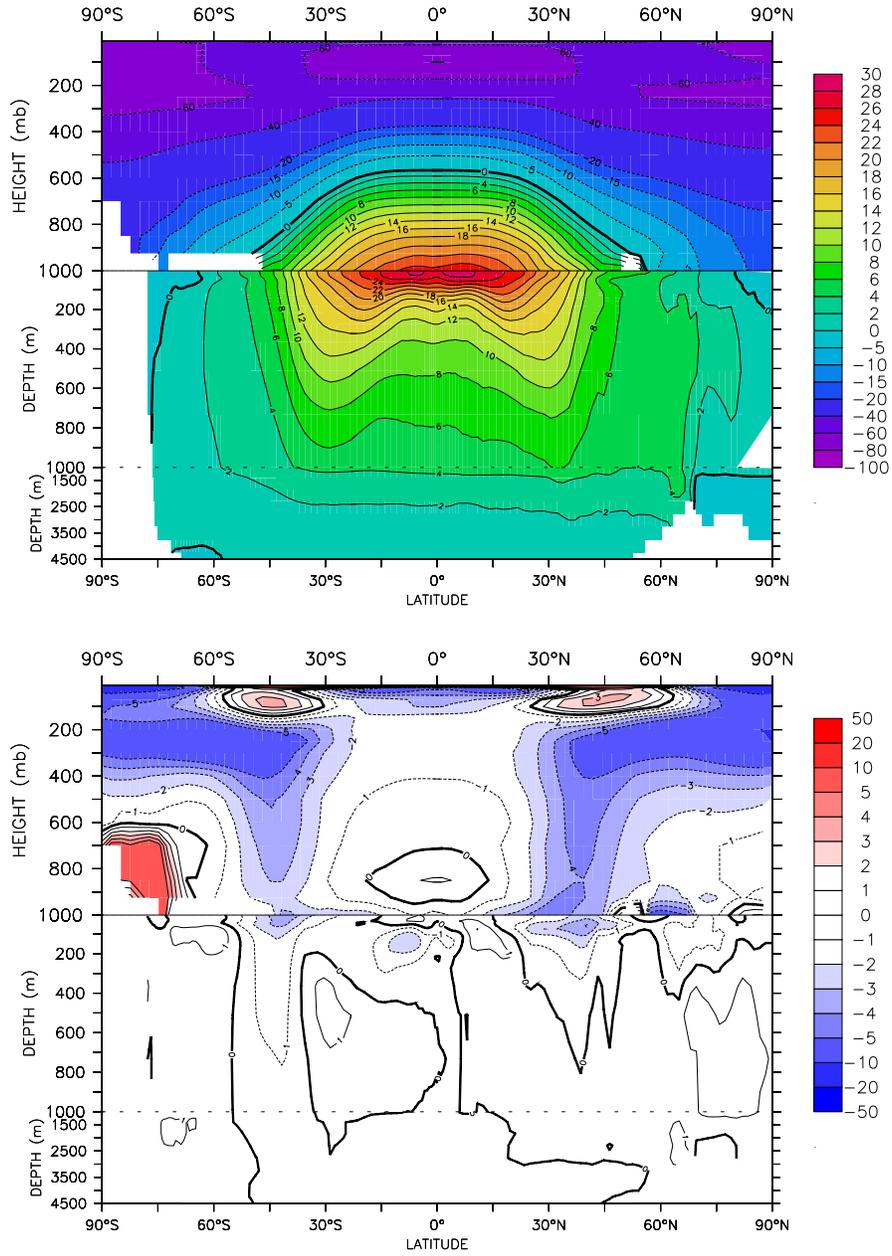
Figure 4.17: Temperature zonal mean: zonal averages of ocean temperature and air temperature. 2L20, years 1851-1940. Top: absolute values, contour interval 10°C below)10, then -5, 0, and 2°C above 0. Bottom: difference with climatology, contour interval 1°C around 0, and 5°C elsewhere
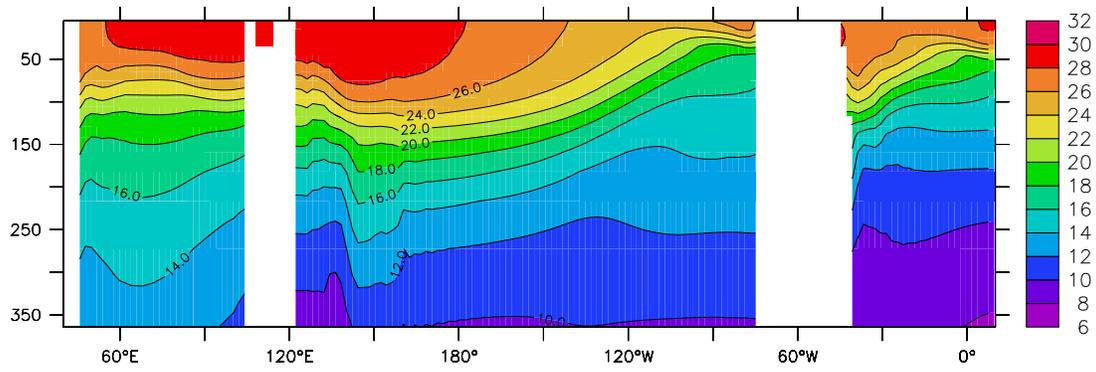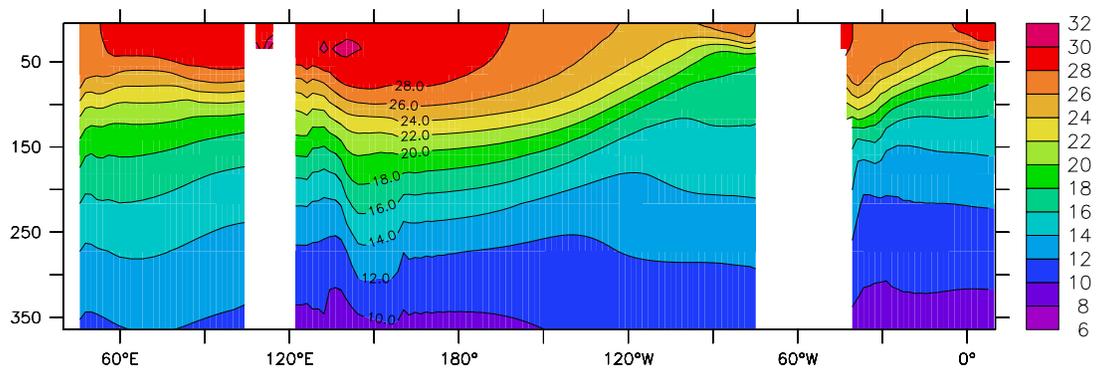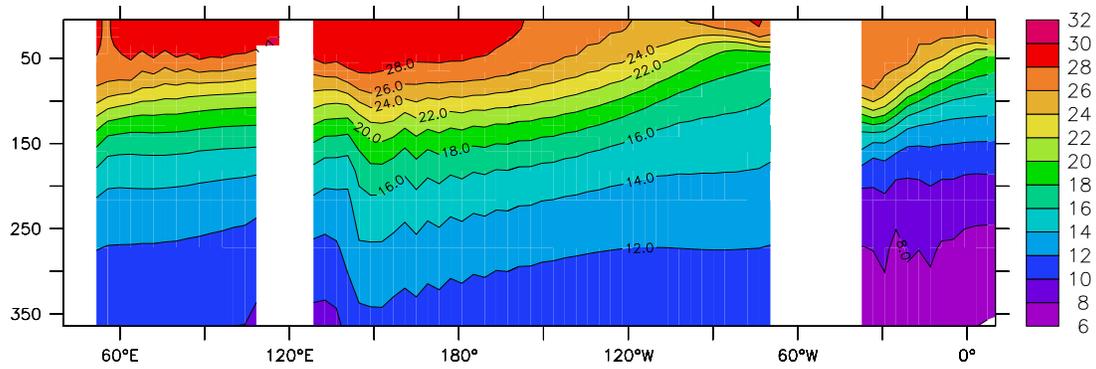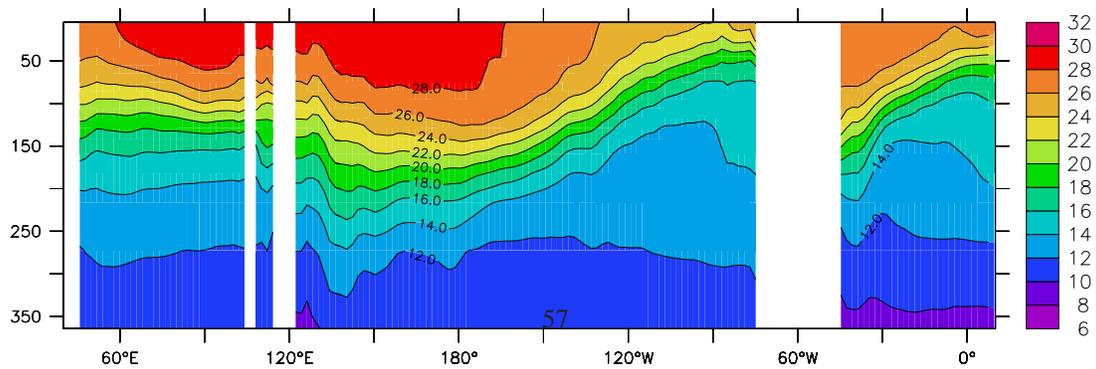
Figure 4.18: Equatorial slice of temperature (0-400m), averaged 2°N-2°S. Contour interval 2°C.

4.3.1 Radiative forcing in the tropical regions

Major improvements in the climatology of the atmospheric model in the tropical regions results from the recent adjustments of the atmospheric model concerning the convection and cloud schemes (see section sec. 2.2.3). Specific care in the development of the cloud scheme was given to the simulation of the cloud radiative forcing in order to get:

- realistic balance between long wave and short wave radiation;

- correct magnitude between summer and winter characteristics in key convective regions;

- realistic balance between regions of deep convection over land and ocean.

Simulation of stratus and stratocumulus type clouds has also been discussed as a key feature of tropical circulation in the eastern part of the ocean basins, and as a major cause of model drawbacks there. These clouds, even though they are crudely represented in the model, are present in the simulation and contribute the radiative forcing. However, they produce too much precipitation compared to reality (fig. 4.8). Results of the atmospheric model show that these adjustments indeed lead to satisfactorily simulation of the cloud radiative forcing when compared to satellite data (fig. 4.19).

In order to evaluate the cloud radiative forcing, we use the diagnostics developed by *Bony et al.* (2004). Fig. 4.19 shows that the convective regimes sorted as a function of vertical velocity at $500\ hPa$ follows estimation from *ERA40* and *NCEP* reanalyses. The model has a tendency to overestimate small subsiding regimes. Interestingly, contrary to the distribution of different convective regimes, the coupled model is in better agreement with data than the forced one within the different regimes. This is particularly true in regions of deep convection ($\omega < 50hPa/s$) where both long wave and shortwave radiative forcings are better simulated. For the net radiative forcing, the larger disagreement ocurs for moderated convective regimes ($-50hPa/s < \omega < 50hPa/s$). Thanks to this features, the zonal mean radiative forcing is in good agreement with *ERBE* data of radiative forcing at the top of atmosphere (not shown).

4.3.2 Mean seasonal cycle

Seasonal cycle at the equator   An interesting feature of the model simulation is the simulations of the mean seasonal cycle in the tropical regions. Fig. 4.20 compares the mean seasonal cycle of SST averaged between 2N and 2S as a function of longitude across the three tropical basins for 2L20, compared with HadSST climatology. The phase and westward extension of the seasonal cycle in the eastern Pacific are well represented, with a slightly to weak amplitude. In the Atlantic the amplitude maximum is shifted in the west, but still there (fig. 4.20). The figure also shows the seasonal cycle of SST in anomaly (annual mean removed) for all the simulations. Its shows that this features is robust to the small changes in the model, and that shifting to lower resolution model allows us to keep the main features of the seasonal cycle in the tropics.

Seasonal cycle and variability in selected regions   The seasonal phasing of the annual cycle is satisfactorily over most regions in the tropics. We examine the simulation of the mean seasonal cycle in four key regions: northwest Indian (50°E-70°E, 0°-10°N), northeast Indian (90°E-110°E, 10°S-Eq), North Atlantic (60°W-20°W, 10°N-20°N - Nat), South Atlantic (30°S-Eq, 10°S-Eq Sat), Niño 3 (150°W-90°W, 5°S-5°N).

Fig. 4.21 shows that all the models best succeed to reproduce the seasonal amplitude of modern SST in the Atlantic, both over NAT and SAT. Models are less successful in the Indian ocean. Data (blue curves) show a semi annual cycle in Indian with one peak in June and a smaller peak in October that is not present in model simulations.

4.4 Known biased and difficulties

Several difficulties concerning the adjustment of the model have been encountered during its development and tuning. Some of the model bias are now documentted, but no solutions have been found yet to improve these aspects of the climatology.
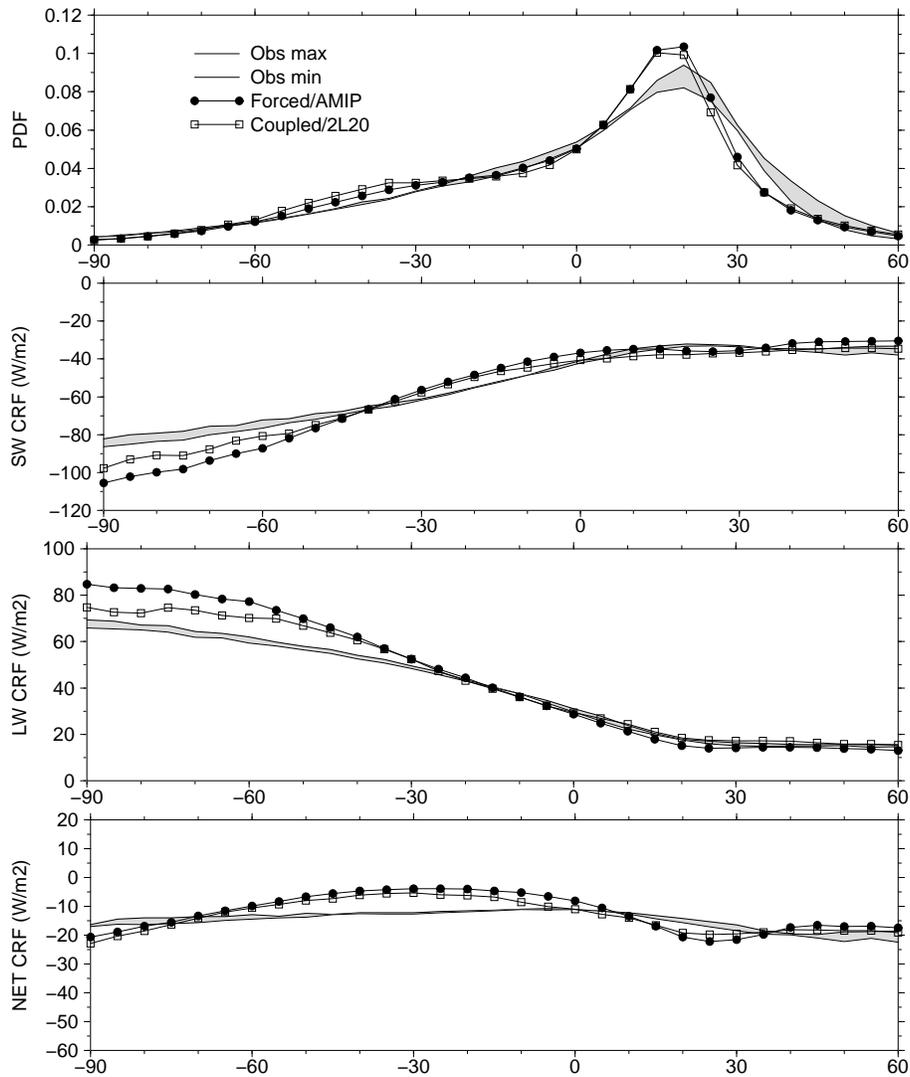
Figure 4.19: Cloud radiative forcing in the tropics. The figure shows the cloud radiative forcing for the different regimes of vertical velocity in the tropics. *a*: distribution of convective regimes, *b*: short wave radiative forcing, *c*: long wave, *d*: net. Grey: maximum and minimum estimations from observations (vertical velocity from *ERA40* and *NCEP* analyses, cloud radiative from *ERBE* data), circles: result from the atmosphere model alone, forced by observed sea surface temperature (*AMIP* simulation), squares: 2L20 coupled simulation. Further explanation in the text (sec. 4.3.1).
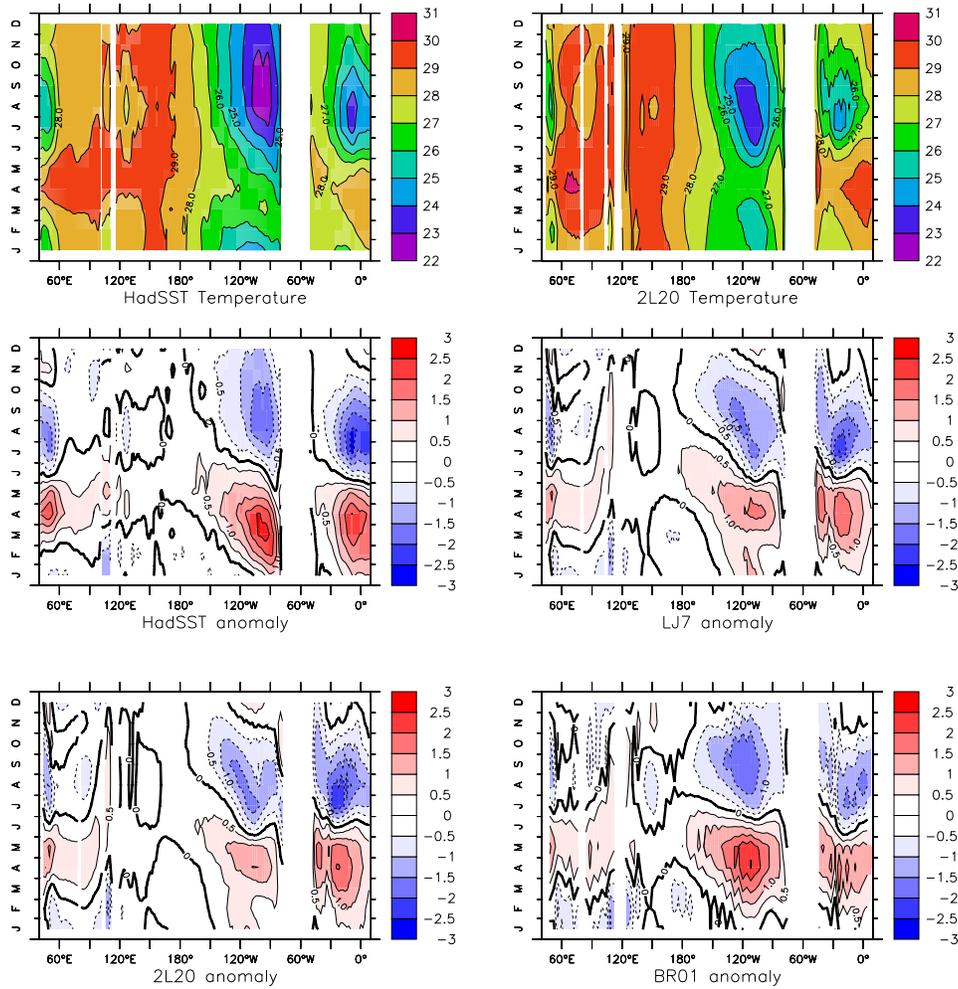
Figure 4.20: Mean seasonal cycle of SST (Celsius), averaged 2°N-2°S. Top Absolute values for observations (HadSST, top left) and 2L20 (top right), with contour interval of 1°C. Middle and bottom: annual mean removed, with contour interval of 0.5°C, for observation (HadSST, middle left), LJ7 (middle, rioght), 2L20 (bottom, left) and BR01 (bottom, right).
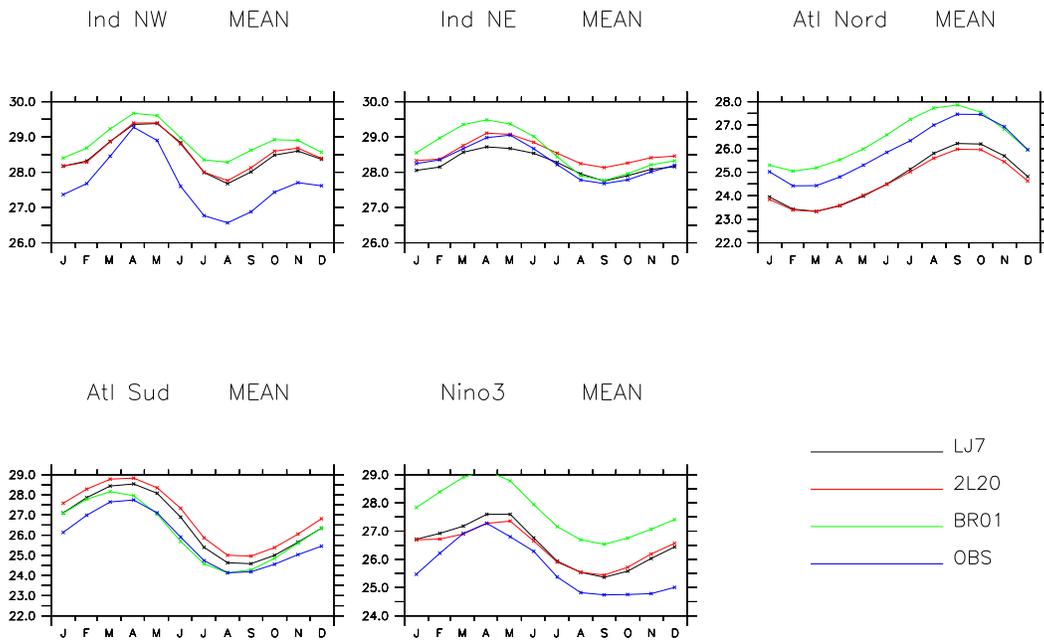
Figure 4.21: Mean seasonal cycle of SST (Celsius) over selected regions: northwest Indian (50°E-70$circ$E, 0°-10°N), northeast Indian (90°E-110°E, 10°S-Eq), North Atlantic (60°W-20°W, 10°N-20°N), South Atlantic (30°S-Eq, 10°S-Eq), Niño 3 (150°W-90°W, 5°S-5°N).
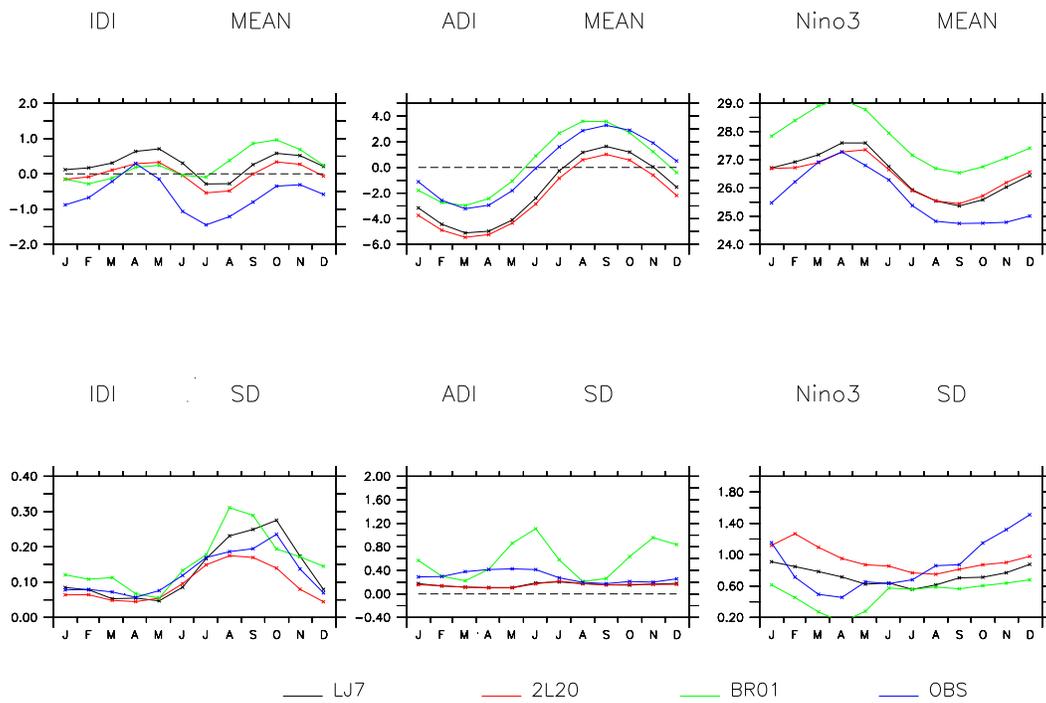
Figure 4.22: Tropical indexes. Top : mean seasonal cycle, bottom: standard deviation to the mean seasonal cycle).
Left: northwest Indian minus northeast Indian, middle: North Atlantic minus South Atlantic, right: Niño 3
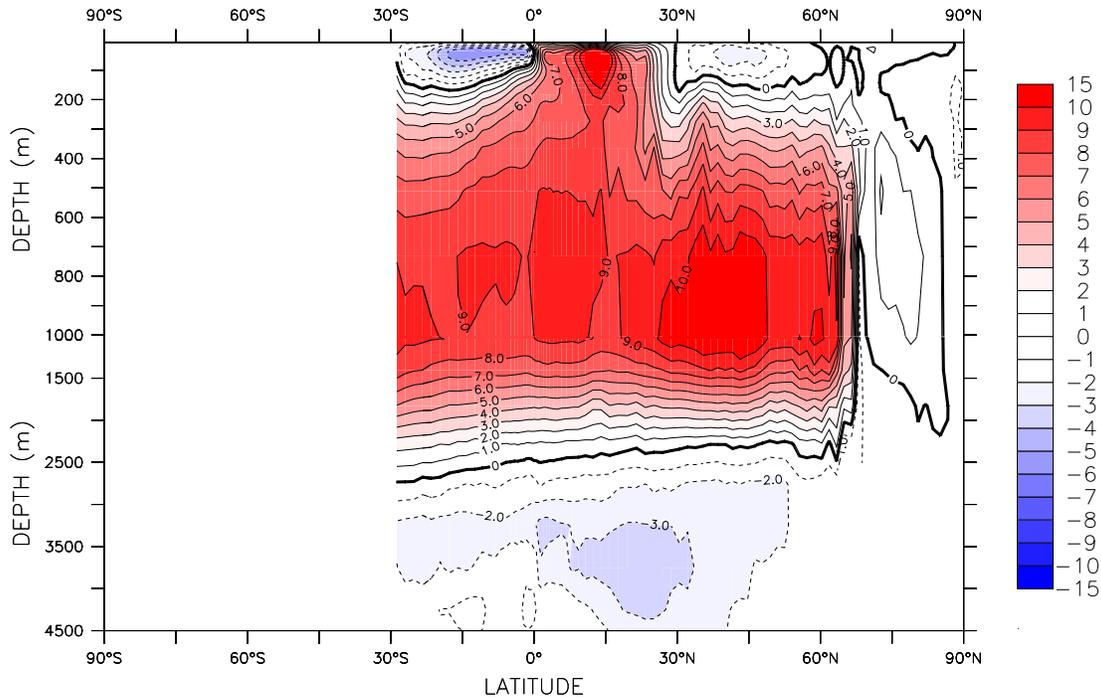
Figure 4.23: Atlantic meridional stream function, LJ7

4.4.1 Monsoon

In this version of the model, the inland extension of the monsoon flow during summer is poorly represented. There is several explanations: (i) there is a cold bias over Hymalaya, mainly due to a late summer warning, yielding to an Indian monsoon shifted to the southeast, (ii) a dry soil in the sub-Saharian region and north of India, yielding to a monsoon through located too far south in Africa (iii) The sea-surface temperature pattern in the Atlantic (too cold north of the equator, and too warm south of if) induces a southward position of the ITCZ which prevents the northward migration of the ITCZ during the boreal summer.

4.4.2 Mid and high latitudes

One of the major bias of this model version is the cold region in mid and high latidudes. It corresponds to an equatorward shift of the stormtrack en mid latitudes. This feature is already present in atmosphere alone simulations and amplifies with the coupling. The resolution of the atmospheric component could be at the origin of the problem. Simulations at higher resolution of the atmosphere alone model show a luch better representation of this features.

4.4.3 Ocean overtuning

In all simulations, the Atlantic meridional circulation has an upper cell, corresponding aproximativly to North Atlantic Deep Water (NADW), to weak compared to data (*Ganachaud and Wunsch*, 2000). As mention when discussing precipitation, the excess precipitation in high latitudes could be at the origine of the strong halocline in the Labrador sea. In this region sea ice expends to much, and deep convection is suppressed. However in the Greenland-Icelandic-Norwegian seas, the model behaviour is satisfactorily.
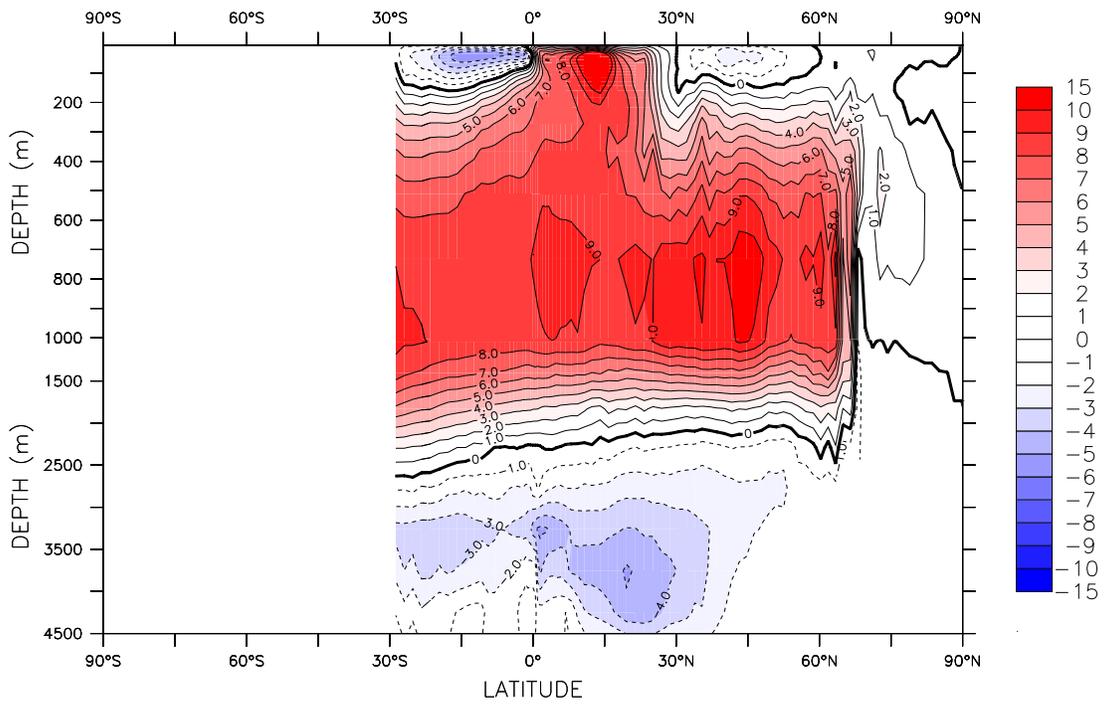
Figure 4.24: Atlantic meridional stream function, 2L20
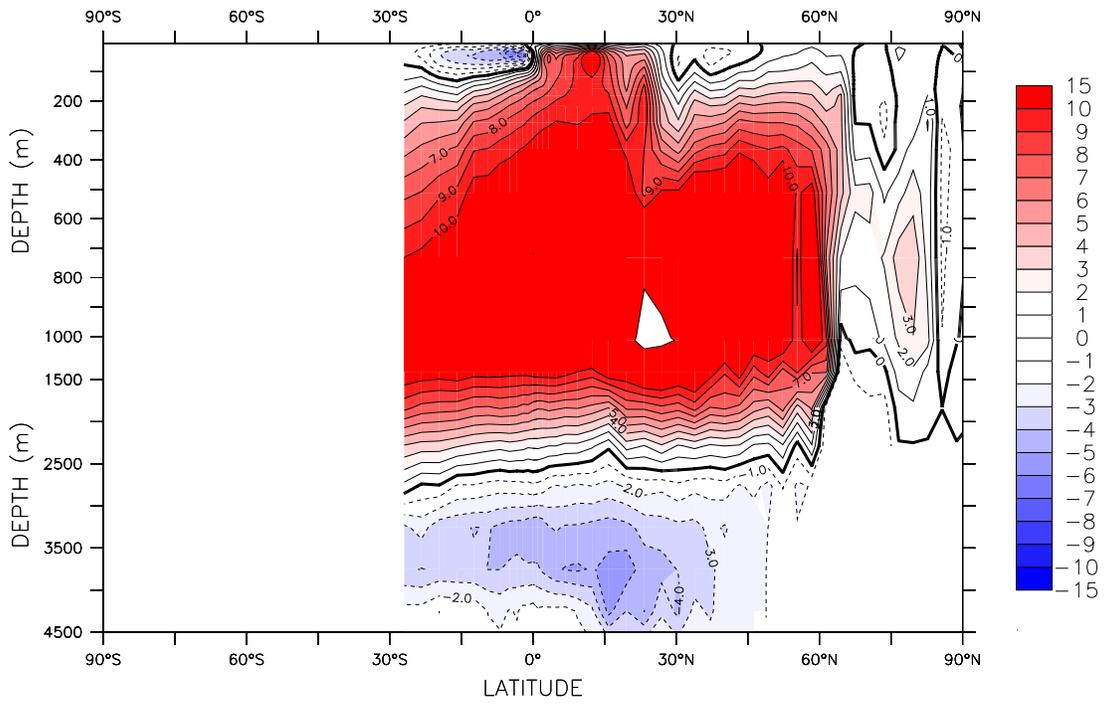
Figure 4.25: Atlantic meridional stream function, BR01
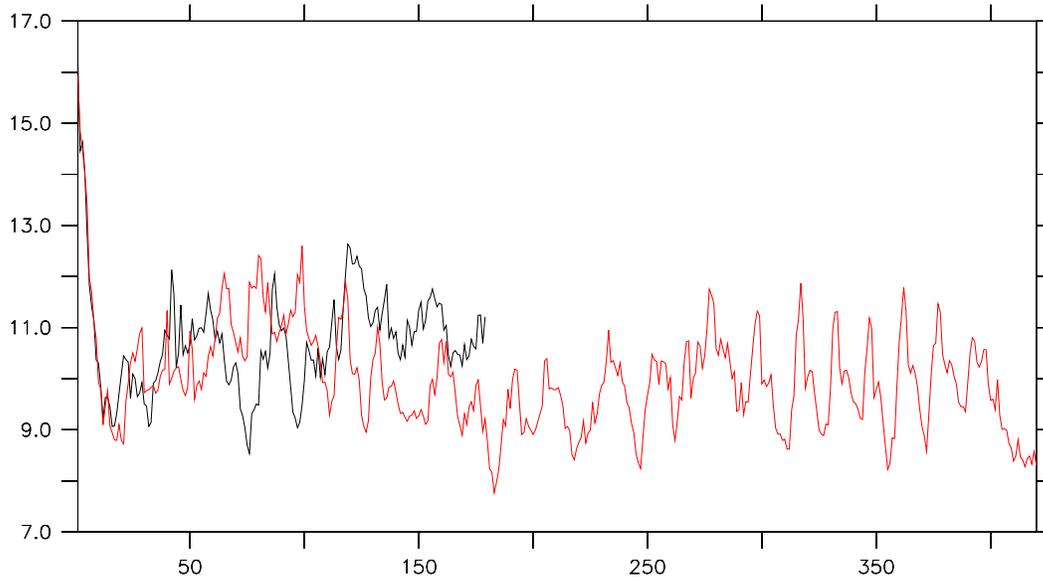
Figure 4.26: Evolution of the maximum of the overturning stream function in the Atlantic for LJ7 (black) and 2L20 (red).

Chapter 5

Acknowledgments

Appendix A

Glossary

List of useful and cryptic terms used in this report.

AGCM Atmospheric General Circulation Model.

AMIP Atmospheric Model Intercomparison project. http://www-pcmdi.llnl.gov/amip/amiphome.html.

ASTR Institut d'Astronomie et de Géophysique Georges Lemaître. An institute of UCL. See http://www.astr.ucl.ac.be.

CCRT Centre de Calcul de la Recherche et de la Technologie. Super computing center of the CEA for its civilian applications.

CEA Commissariat l'Energie Atomique. The french nuclear energy agency. http://www.cea.fr.

CERFACS European Center for Research and Advanced Training in Scientific Computation. See www.cerfacs.fr.

CGCV Centre Grenoblois de Calcul Vectoriel. Former super computing center of the CEA, closed in October 2003.

CLIO OGCM of the UCL/ASTR.

CLIVAR An international research program on climate variability and predictability. A program of *WMO/WCRP*. http://www.clivar.org/.

CMIP Coupled Models Intercomparison Project. . http://www-pcmdi.llnl.gov/cmip.

CNRS Centre National de la Recherche Scientifique. http://www.cnrs.fr.

CVS Concurrent Versions System, the dominant open-source network-transparent version control system. http://www.cvshome.org.

DODS Former name of the *OPeNDAP* protocol.

ECHO Evaluation des modèles Couplés au moyen HOlocène. A research program of *PNEDC* coordinated by Pascale Braconnot (CEA) and Bruno Turq (IRD).

ECMWF European Center for Medium-Range Weather Forecast. http://www.ecmwf.int.

ERA40 ECMWF Re-Analysis. http://www.ecmwf.int/research/era

ENSIP A coordinated study to compare the simulations of ENSO in coupled ocean-atmosphere models, organized by GOALS Numerical Experimentation Group (NEG1) of Climate Variability and Predictability (CLIVAR). Coordinator: M. Latif (Max-Planck-Institut für Meteorologie). http://www.clivar.org/organization/wgsip/projects/ensip.htm.

FAST-ATLAS Collection of *Ferret* and `Ksh` scripts designed to facilitate layout and creation of diagnotics. A description of this framework is available at http://dods.ipsl.jussieu.fr/fast

Ferret An interactive computer visualization and analysis environment designed to meet the needs of oceanographers and meteorologists analyzing large and complex gridded data sets. It runs on most Unix systems (including Linux and MacOSX), and on Windows NT/9x using X windows for display. It can be installed to run from a Web browser ("WebFerret") for use while away from your desk or from a system lacking X windows software. It can transparently access extensive remote Internet data bases using OPeNDAP (formerly known as DODS). http://www.unidata.ucar.edu/packages/dods.

FSCINT Bicubic interpolation library of *OASIS*.

IDRIS Institut du Développement et des Ressources en Informatique Scientitique. Super computing center of the CNRS. http://www.idris.fr.

IOIPSL Input/Output software libray developped at IPSL, and used in all components of the coupled model.

IPSL Institut Pierre Simon Laplace des sciences de l'environnement. A federation of six laboratories in environnemental sciences: *LSCE*, *LOCEAN*, *LMD*, *SA*, *CETP*. http://www.ipsl.jussieu.fr.

IRD Institut de Recherche pour le Développement. Formerly named ORSTOM. http://www.ird.fr.

ITCZ InterTropical Convergence Zone.

LAI Leaf area index. The ration between the surface of leaves and the surface of ground.

LMD Laboratoire de Météorologie Dynamique. A joint research researhc unit of Ecole Polytechnique, Ecole Normale Supérieure, Université Pierre et Marie Curie and CNRS. An *IPSL* laboratory. http://www.lmd.jussieu.fr.

LODYC Laboratoire d'Océanographie DYnamique et de Climatologie. A joint research unit of CNRS, IRD (ex-ORSTOM) and Université Pierre et Marie Curie. An *IPSL* laboratory. . http://www.lodyc.jussieu.fr. Recently merged with *LBCM* to form *LOCEAN*.

LOCEAN A joint research unit of CNRS, IRD (ex-ORSTOM) and l'Université Pierre et Marie Curie. An *IPSL* laboratory. Result of the merger between *LODYC* and *LBCM*. http://www.lodyc.jussieu.fr

LSCE Laboratoire des Sciences du Climat et de l'Environnement. A joint research unit of CEA and CNRS. An *IPSL* laboratory. http://www.lsce.cnrs-gif.fr.

LIM Louvain Ice Model. Dynamic and thermodynamic sea-ice model developed by *UCL/ASTR*.

LOA Laboratoire d'Optique Atmosphérique. A joint research unit of CNRS (UMR 1518) and Université des sciences et technologies de Lille. http://loasys.univ-lille1.fr

MODIPSL Software infractructure of the IPSL coupled model.

MOSAIC Software package to compute interpolation weights.

MOTIF Model and Observation to Test clImate Feedbacks. A project funded by the 5th Framework Program of the European Union, under number EVK2-2001-00263. http://www-lsce.cea.fr/motif.

MOZAIC Interpolation library of *OASIS*. It uses weights provided by the user.

MPI Message Passing Interface. http://www-unix.mcs.anl.gov/mpi.

NADW North Atlantic Deep Water.

NCEP National Center for Environmental Prediction, United States. http://www.ncep.noaa.gov.

NEMO Ocean general circulation model developped at *LOCEAN*, previously known as :*OPA*. http://www.lodyc.jussieu.fr/NEMO.

NetCDF Network Common Data Format. Interface for array-oriented data access and a library that provides an implementation of the interface. The netCDF library also defines a machine-independent format for representing scientific data. http://www.unidata.ucar.edu/packages/netcdf.

OGCM Ocean general Circulation Model.

OASIS Ocean Atmosphere Sea-Ice Soil. The coupler used in IPSL_CM4. Developed by CERFACS. http://www.cerfacs.fr/globc/softwa

OPA Ocean general circulation model developped at *LOCEAN*. http://www.lodyc.jussieu.fr/opa. *OPA* has been recently renamed as *NEMO*.

OPeNDAP A protocol formerly known as DODS, the Distributed Oceanographic Data System. It allows users to access data anywhere from the internet using a variety of client/server methods, including Ferret. Employing technology similar to that used by the World Wide Web, DODS and Ferret create a powerful tool for the retrieval, sampling, analyzing and displaying of datasets; regardless of size or data format (though there are data format limitations). Full documention at http://www.unidata.ucar.edu/packages/dods.

ORCA Configuration of *OPA* with a grid covering the whole globe. Presently, three resolutions exist: ORCA4 (4 degree grid), ORCA3 (2 degree grid) and ORCA05 (0.5 degrees grid). The two first are coupled with LMDZ.

ORCHIDEE ORganizing Carbon and Hydrology In Dynamic EcosystEms. ORCHIDEE is the new land-surface scheme of the IPSL. This scheme is the result of the coupling of the SECHIBA land-surface scheme, which is dedicated to the surface energy and water balances, and the carbon and vegetation model STOMATE. As the model goes into the production phase we will have more time to dedicate to the documentation and this web page. http://www.ipsl.jussieu.fr/~ssipsl.

ORSTOM Former name of *IRD*.

PAGES PAst Global changES. Core international program initated by the International Geosphere-Biosphere Program (IGBP).

PFT Plant functional types. A PFT groups species with similar characteristics in a way which maximise the potential to predict accurately the responses of real vegetation with real species diversity.

PMIP Paleoclimate Modelling Intercomparison Project. An international project sponsored by Pages and CLIVAR. http://www-lsce.cea.fr/pmip2.

PNEDC Programme National d'Etude du Climat. A research program of CNRS.

PRISM Program for Integrated Earth System Modeling. An Infrastructure Project for Climate Research in Europe funded be the European Commission under contract number EVR1-CT-2001-40012. http://prism.enes.org.

SA Service d'Aéronomie. A joint research unit (UMR 7620) of *CNRS*, Université Pierre et Marie Curie and Université Versailles-Saint-Quentin. An *IPSL* laboratory. . http://www.aero.jussieu.fr.

SPCZ South Pacific Convergence Zone.

STOIC Study of Tropical Oceans In Coupled models. A *WCRP/CLIVAR* programme, within *GOALS-NEG1* (Numerical Experimentation Group). An intercomparison of tropical ocean behaviour in coupled ocean-atmosphere models, on seasonal and interannual timescales, focussing on the Atlantic and Indian regions and to investigate the relationship to the Pacific region. Coordinated by Michael Davey (*UKMO*). http://www.clivar.org/organization/wgsip/projects/s

UCL Université Catholique de Louvain-la-Neuve. . http://www.ucl.ac.be.

WCRP World Climate Research Program. A program of the World Meteorological Organisation. http://www.wmo.ch/web/wcrp/wcrp-h

WMO World Meteorological Organization. http://www.wmo.ch.

Hope this helped!

Appendix B

Interpolations

B.1 Wind stress interpolations

B.1.1 General relationship between vectors

- $\vec{a} = +cos(\lambda)\vec{x} + sin(\lambda)\vec{y}$, $\vec{n} = -sin(\phi)\vec{a} + cos(\phi)\vec{z}$, $\vec{k} = +cos(\phi)\vec{a} + sin(\phi)\vec{z}$

- $\vec{e} = -sin(\lambda)\vec{x}$

- $\vec{n} = -sin(\phi)cos(lambda)\vec{x} - sin(\phi)sin(lambda)\vec{z} + cos(\phi)\vec{z}$

- $\vec{k} = -cos(\phi)cos(lambda)\vec{x} - cos(\phi)sin(lambda)\vec{z} + sin(\phi)\vec{z}$

- $\vec{i} = +cos(\alpha)\vec{e} + sin(\alpha)\vec{n}$, $\vec{e} = +cos(\alpha)\vec{i} - sin(\alpha)\vec{j}$

- $\vec{j} = -sin(\alpha)\vec{e} + cos(\alpha)\vec{n}$, $\vec{e} = +cos(\alpha)\vec{i} - sin(\alpha)\vec{j}$

- $\vec{a} = -sin(\phi)\vec{n} + cos(\phi)\vec{k}$, $\vec{x} = -sin(\lambda)\vec{e} + cos(\lambda)\vec{a}$, $\vec{y} = -cos(\lambda)\vec{e} + sin(\lambda)\vec{a}$

- $\vec{x} = -sin(\lambda)\vec{e} - cos(\lambda)sin(\phi)\vec{n} + cos(\lambda)cos(\phi)\vec{k}$

- $\vec{y} = +cos(\lambda)\vec{e} - sin(\lambda)sin(\phi)\vec{n} + sin(\lambda)cos(\phi)\vec{k}$

- $\vec{z} = +cos(\phi)\vec{n} + sin(\phi)\vec{k}$

Wind stress is defined in the atmosphere model by $\vec{t} = t_i\vec{e} + t_j\vec{n} + \left[t_k\vec{k}\right]$. Last term (vertical) is null.

- $t_e = -sin(\lambda)t_x + cos(\lambda?)t_y$

- $t_n = -cos(\lambda)sin(\phi)t_x - sin(\lambda)sin(\phi)t_y + cos(?)t_z$

- $t_k = +cos(\lambda)cos(\phi)t_x + sin(\lambda)cos(\phi)t_y + sin(\phi?)t_z$

The components are interpolated toward the ocean in the esatward/northward referential. The last step consists to compute the component in the referential of the *ORCA model*

- $t_e = -sin(\lambda)t_x + cos(\lambda)t_y$

- $t_n = -cos(\lambda)sin(\phi)t_x - sin(\lambda)sin(\phi)t_y + cos(\phi)t_z$

- $t_k = +cos(\lambda)cos(\phi)t_x + sin(\lambda)cos(\phi)t_y + sin(\phi)t_z$

Bibliography

Ball, J., T. Woodrow, and J. Berry, A model predicting stomatal conductance and its contribution to the control of photosynthesis under different environmental conditions, *Progress in Photosynthesis*, *4*, 221–224, 1987.

Barthelet, P., Transient CO_2 experiment using the ARPEGE/OPAICE non flux corrected coupled model, *Geophys. Res. Lett.*, *25*, 2277–2280, 1998.

Beckman, A., The representation of bottom boundary layer processes in numerical ocean circulation models, in *Ocean Modeling and Parametrization*, edited by E. P. Chassignet and J. Verron, Kluwer Acad., Norwell, Mass., 1998.

Berthelot, M., P. Friedlingstein, P. Ciais, P. Monfray, J.-L. Dufresne, H. Le Treut, and L. Fairhead, Interactions between future climate changes and carbon cycle on land, *Global Biogeochemical Cycles*, 2002.

Blanke, B., and P. Delecluse, Variability of the tropical Atlantic ocean simulated by a general circulation model with two mixed layer physics, *Journal of Physical Oceanography*, *23*, 1363–1388, 1993.

Bony, S., and K. A. Emmanuel, A parameterization of the cloudiness associated with cumulus convection; evaluation using TOGA COARE data, *J. Atmos. Sci.*, *58*, 3158–3183, 2001.

Bony, S., and H. Le Treut, Validation of GCM-simulated annual cycle of the Earth radiation budget an cloud forcing, *J. Geophys. Res.*, *96*, 18,061–18,081, 1992.

Bony, S., J.-L. Dufresne, H. Le Treut, J.-J. Morcrette, and C. Senior, On dynamic and thermodynamic components of cloud changes, *Clim. Dyn.*, *22*, 71–86, 2004.

Bopp, L., P. Monfray, O. Aumont, J.-L. Dufresne, H. Le Treut, G. Madec, L. Terray, and J. C. Orr, Potential impact of climate change on marine export production, *Global Biogeochemical Cycles*, *15*, 81–99, 2001.

Bopp, L., K. Kohfeld, C. Le Quéré, and O. Aumont, Dust impact on marine biota and atmospheric CO_2 during glacial periods, *Paleoceanography*, *18*, 2003.

Botta, A., N. Viovy, P. Ciais, and P. Friedlingstein, A global prognostic scheme of leaf onset using satellite data, *Glob. Change Biol.*, *6*, 709–726, 2000.

Braconnot, P., Adjustment and feedbacks in a global coupled ocean-atmosphere model, *Clim. Dyn.*, *13*, 507–519, 1997.

Braconnot, P., Tests de sensibilité, *Note technique 0076*, IPSL, 1998.

Braconnot, P., and O. Marti, Impact of precession on monsoon characteristics from coupled ocean atmosphere experiments: changes in Indian monsoon and Indian ocean climatology, *Marine Geology*, *201(1-3)*, 23–34, 2003.

Braconnot, P., S. Joussaume, O. Marti, and N. Noblet, Synergistic feedbacks from ocean and vegetation on the african monsoon response to mid-Holocene insolation, *Geophys. Res. Lett.*, *26(16)*, 2481–2484, 1999.

Braconnot, P., O. Marti, S. Joussaume, and Y. Leclainche, Ocean feedback in response to 6 kyr BP insolation, *Clim. Dyn.*, *13(9)*, 1537–1553, 2000.

Braconnot, P., S. Harrison, S. Joussaume, C. Hewitt, A. Kitoh, J. Kutzbach, Z. Liu, B. L. Otto-Bleisner, J. Syktus, and S. L. Weber, Evaluation of coupled ocean-atmosphere simulations of the mid-Holocene, *in press*, 2004.

Collatz, G., M. Ribas-Carbo, and J. Berry, Coupled photosynthesis-stomatal conductance model for leaves of C_4 plants, *Aust. J. Plant Physiol*, *19*, 519–538, 1992.

Davey, M. K., M. Huddleston, K. R. Sperber, P. Braconnot, F. Bryan, D. Chen, A. Colman, C. Cooper, U. Cubasch, P. Delecluse, D. De Witt, L. Fairhead, G. Flato, C. Gordon, T. Hogan, M. Ji, M. Kimoto, A. Kitoh, T. Knutson, M. Latif, H. Le Treut, T. Li, S. Manabe, C. Mechoso, G. A. Meehl, J. Oberhüber, S. Power, E. Roeckner, L. Terray, A. Vintzileos, R. Voss, B. Wang, B. M. Washington, I. Yoshikawa, J.-Y. Yu, and. Yukimoto, and S. Zebiak, STOIC: a study of coupled model climatology and variability in tropical ocean regions, *Clim. Dyn.*, *18*, 403–420, 2002.

De Rosnay, P., J. Polcher, K. Laval, and M. Sabre, Integrated parameterization of irrigation in the land surface model orchidee. validation over indian peninsula, *Geophys. Res. Let.*, *30(19)*, doi:10.1029/2003GL018024, 2003.

Ducoudré, N., K. Laval, and A. Perrier, SECHIBA, a new set of parameterizations of the hydrologic exchanges at the land-atmosphere interface within the LMD atmospheric general circulation model, *Clim. Dyn.*, *6*, 248–273, 1993.

Dufresne, J.-L., and J.-Y. Grandpeix, Raccordement des modèles thermodynamiques de glace, d'océan et d'atmosphère, *Note Interne 205*, L.M.D., 1996.

Dufresne, J.-L., P. Friedlingstein, M. Berthelot, L. Bopp, L. Fairhead, H. Le Treut, and P. Monfray, On the magnitude of positive feedback between future climate change and the carbon cycle, *Geophys. Res. Lett.*, *29*, 2002.

Emanuel, K. A., A scheme for representing cumulus convection in large-scale models, *J. Atmos. Sci.*, *48*, 2313–2335, 1991.

Farquhar, G., S. von Caemmener, and J. Berry, A biochemical model of photosynthesis CO_2 fixation in leaves of C_3 species, *Planta*, *49*, 78–90, 1980.

Fichefet, T., and M. A. Morales Maqueda, Sensitivity of a global sea ice model to the treatment of ice thermodynamics and dynamics, *J. Geophys. Res.*, *102*, 2609–12,646, 1997.

Fichefet, T., and M. A. Morales Maqueda, Modelling the influence of snow accumulation and snow-ice formation on the seasonal cycle of the Antarctic sea-ice cover, *Clim. Dyn.*, *15*, 251–268, 1999.

Filiberti, M.-A., J.-L. Dufresne, and J.-Y. Grandpeix, Reference manual for IGLOO sea ice model., *Note technique du Pôle de modélisation*, Institut Pierre-Simon Laplace, 2001.

Forget, F., F. Hourdin, R. Fournier, C. Hourdin, O. Talagrand, M. Collins, S. R. Lewis, P. L. Read, and J.-P. Huot., Improved general circulation models of the Martian atmosphere from the surface to above 80 km, *J. Geophys. Res.*, *104*, 24,155–24,176, 1999.

Fouquart, Y., and B. Bonnel, Computations of solar heating of the Earth's atmosphere: a new parametrization, *Beitr. Phys. Atmos.*, *53*, 35–62, 1980.

Friedlingstein, P., J. Guïot, C. B. Field, and I. Y. Fung, Toward an allocation scheme for global terrestrial carbon models, *Glob. Change Biol.*, *5*, 755–770, 1999.

Friedlingstein, P., L. Bopp, P. Ciais, J.-L. Dufresne, L. Fairhead, H. Le Treut, P. Monfray, and J. Orr, Positive feedback between future climate change and the carbon cycle, *Geophys. Res. Letters*, *28*, 1543–1546, 2001.

Friedlingstein, P., J.-L. Dufresne, P. Cox, and P. Rayner, How positive is the feedback between climate change and the carbon cycle?, *Tellus*, *55B*, 692–700, 2003.

Ganachaud, A., and C. Wunsch, Improved estimates of global ocean circulation, heat transport and mixing from hydrographic data, *Nature*, *408*, 453–457, 2000.

Gloersen, P., and W. Campbell, Recent variations in Arctic and Antarctic sea-ice covers, *Nature*, *352*, 33–36, 1991.

Grenier, H., Les interactions air-mer dans le système climatique: étude à l'aide d'un modèle couplé tri-dimensionnel océan-atmosphère-glace marine, Ph.D. thesis, Université Catholique de Louvain-la-Neuve, 1997.

Grenier, H., H. Le Treut, and T. Fichefet, Ocean-atmosphere interactions and climate drift in a coupled general circulation model, *Climate Dynamics*, *16*, 701–717, 2000.

Guilyardi, E., G. Madec, and L. Terray, The role of lateral ocean physics in the upper ocean thermal balance of a coupled ocean-atmosphere GCM, *Clim. Dyn.*, *17*, 589–599, 2001.

Hagemann, S., and L. Dümenil, A parametrization of the lateral waterflow on the global scale, *Clim. Dyn.*, *14*, 17–31, 1998.

Hibler, W. I., A dynamic thermodynamic sea ice model, *J. Phys. Oceanogr.*, *9*, 815–846, 1979.

Hourdin, F., and A. Armengaud, Test of a hierarchy of finite-volume schemes for transport of trace species in an atmospheric general circulation model, *Mon. Wea. Rev.*, *127*, 822–837, 1999.

Hourdin, F., P. Le Van, F. Forget, and O. Talagrand, Meteorological variability and the annual surface pressure cycle on Mars, *J. Atmos. Sci.*, *50*, 3625–3640, 1993.

Hourdin, F., O. Talagrand, R. Sadourny, C. Régis, D. Gautier, and C. P. McKay, General circulation of the atmosphere of Titan, *Icarus*, *117*, 358–374, 1995.

IPCC, *Climate Change 2001, The Scientific Basis*, 98 pp., Cambridge University press, 2001.

Khodri, M., Y. Le Clainche, G. Ramstein, P. Braconnot, O. Marti, and E. Cortijo, Simulating the amplification of orbital forcing by ocean feedbacks in the last glaciation, *Nature*, *410*, 570–574, 2001.

Krinner, G., C. Genthon, and al., Studies of the antarctic climate with a stretched-grid general circulation model, *Journal of Geophysical Research*, *102*, 13,731–13,745, 1997.

Krinner, G., N. Viovy, N. de Noblet-Ducoudré, J. Ogée, J. Polcher, P. Friedlingstein, P. Ciais, S. Sitch, and C. Prentice, A dynamic global vegetation model for studies of the coupled atmosphere-biosphere system, *Glob. Biogeochem. Cyc.*, *19*, GB1015, doi:10.1029/2003GB002199, 2005.

Latif, M., K. Sperber, J. Arblaster, P. Braconnot, D. Chen, A. Colman, U. Cubasch, C. Cooper, P. Delecluse, D. DeWitt, L. Fairhead, G. Flato, T. Hogan, M. Ji, M. Kimoto, A. Kitoh, T. Knutson, H. Le Treut, T. Li, S. Manabe, O. Marti, C. Mechoso, G. Meehl, S. Power, E. Roeckner, J. Sirven, L. Terray, A. Vintzileos, R. Voss, B. Wang, W. Washington, I. Yoshikawa, J. Yu, and S. Zebiak, ENSIP: the El Niño simulation intercomparison, *Clim. Dyn.*, *18*, 255–276, 2001.

Laurent, C., Variabilité climatique basse-fréquence simulée en Atlantique nord par un modèle couplé océan-atmosphère, Ph.D. thesis, Physique de l'environnement. Paris, Université Paris VI, 2000.

Laval, K., R. Sadourny, and Y. Serafini, Land surface processes in a simplified general circulation model, *Geophys. Astrophys. Fluid Dyn.*, *17*, 129–150, 1981.

Le Clainche, Y., Modélisation du ruissellement dans un modèle couplé océan-atmosphère, *Tech. rep.*, LSCE, 1996.

Le Clainche, Y., P. Braconnot, and al., Role of sea-ice thermodynamic in the northern hemisphere climate simulated by a coupled ocean-atmosphere-sea ice model, *Note du Pôle de modélisation 21*, Institut Pierre-Simon Laplace, 2001.

Le Treut, H., and Z. X. Li, Sensitivity of an atmospheric general circulation model to prescribed SST changes: feedback effects associated with the simulation of cloud optical properties, *Climate Dynamics*, *5*, 175–187, 1991.

LeClainche, Y., Etude du couplage océan-glace-atmosphère et de l'impact de la glace de mer sur le climat des hautes latitudes, Ph.D. thesis, Océanologie, Météorologie et Environnement. Paris, Université Paris 6, 2000.

Levitus, S., Climatological atlas of the world ocean, *Professional paper*, NOAA/GFDL, 1982.

L'Heveder, B., Variabilité saisonnière et interannuelle des glaces de mer en Arctique: influence des interactions avec l'atmophère, Ph.D. thesis, Thèse de Doctorat mention Océanographie, Météorologie et Environnement, Paris VI, 1999.

Li, Z. X., and S. Conil, A 1000-year simulation with the IPSL ocean-atmosphere coupled model, *Annals of Geophysics*, *46(1)*, 39–46, 2003.

Lott, F., Alleviation of stationary biases in a GCM through a mountain drag parametrization scheme and a simple representation of mountain lift forces, *Mon. Wea. Rev.*, *127*, 788–801, 1999.

Lott, F., and M. Miller, A new sub-grid scale orographic drag parametrization: its formulation and testing., *Q. J. R. Meteorol. Soc.*, *123*, 101–128, 1997.

Louis, J.-F., A parametric model of vertical eddy fluxes in the atmosphere., *Boundary-layer Meteorol.*, *17*, 187–202, 1979.

Madec, G., and M. Imbard, A global ocean mesh to overcome the north pole singularity, *Climate Dynamics*, *12(6)*, 381–388, 1996.

Maes, C., G. Madec, and P. Delecluse, Sensitivity of an equatorial Pacific OGCM to the lateral diffusion, *Monthly Weather Review*, *125*, 958–971, 1997.

Miller, M. J., A. C. M. Beljaars, and T. N. Palmer, The sensitivity of the ECMWF model to the parameterization of evaporation from the tropical oceans, *J. of Clim.*, *5*, 418–435, 1992.

Morcrette, J.-J., L. Smith, and Y. Fouquart, Pressure and temperature dependence of the absorption in longwave radiation parametrizations, *Contrib. Atmos. Phys.*, *59*(4), 455–469, 1986.

Murray, R. J., Explicit generation of orthogonal grids for ocean models, *Journal of Computational Physics*, *126*, 251–273(23), 1996.

Ngo-Duc, T., J. Polcher, and K. Laval, 53 years forcing data set for land-surface models, *J. Geophys. Res.*, p. accepted, 2005.

Parton, W. J., J. W. S. Stewart, and C. V. Cole, Dynamics of C, N, P, and S in grassland soil: a model, *Biogeochemistry*, *5*, 109–131, 1988.

Paulson, C. A., and J. J. Simpson, Irradiance measurements in the upper ocean, *J. Phys. Oceanogr.*, *7*, 952–956, 1977.

Polcher, J., B. McAvaney, P. Viterbo, M.-A. Gaertner, A. Hahmann, J.-F. Mahfouf, J. Noilhan, T. Phillips, A. Pitman, C. Schlosser, J.-P. Schulz, B. Timbal, D. Verseghy, and Y. Xue, A proposal for a general interface between land-surface schemes and general circulation models, *Global and Planetary Change*, *19*, 263–278, 1998.

Prather, M. C., Numerical advection by conservation of second-order moments, *J. Geophys. Res.*, *91*, 6671–6681, 1986.

Roullet, G., and G. Madec, Salt conservation, free surface, and varying levels: a new formulation for ocean general circulation models, *J. Geophys. Res.*, *105*, 2000.

Ruimy, A., G. Dedieu, and B. Saugier, TURC: A diagnostic model of continental gross primary productivity and net primary productivity, *Glob. Biogeochem. Cycles*, *10*, 269–285, 1996.

Sadourny, R., and K. Laval, January and July performance of the LMD general circulation model, in *New perspectives in Climate Modeling*, edited by A. Berger and C. Nicolis, Elsevier, pp. 173–197, Elsevier, Amsterdam, 1984.

Sitch, S., B. Smith, I. C. Prentice, A. Arneth, B. A., W. Cramer, J. Kaplan, S. Levis, W. Lucht, M. Sykes, K. Thonicke, and S. Venevsky, Evaluation of ecosystem dynamics, plant geography and terrestrial carbon cycling in the LPJ dynamic global vegetation model, *Global Change Biology*, *9*, 161–185, 2003.

Smith, S. D., Coefficients for sea surface wind stress, heat flux, and wind profiles as a function of wind speed and temperature, *J. Geophys. Res.*, *93*, 15,467–15,472, 1988.

Swingedouw, D., P. Braconnot, P. Delecluse, and O. Marti, Sensitivity of the thermohaline circulation to global fresh-water forcing, in prep.

Terray, L., E. Sevault, E. Guilyardi, and O. Thual, The OASIS coupler user guide version 2.0, *Tech. Rep. TR/CMGC*, CERFACS, 1995.

Tiedtke, M., A comprehensive mass flux scheme for cumulus parameterization in large-scale models, *Mon. Wea. Rev.*, *117*, 1179–1800, 1989.

Van Leer, B., Towards the ultimate conservative difference scheme: IV. A new approach to numerical convection, *J. Computational Phys.*, *23*, 276–299, 1977.

Verant, S., K. Laval, J. Polcher, and M. Castro, Sensitivity of the continental hydrological cycle to the spatial resolution over the iberian peninsula, *J. of Hydrometeorology*, *5(2)*, 267–285, 2003.

Vintzileos, A., P. Delecluse, and R. Sadourny, On the mechanisms in a tropical ocean-global atmosphere coupled general circulation model. part i: mean state and the seasonal cycle, *Clim. Dyn.*, *15*, 43 – 62, 1999.

WCRP-111, WMO/TD-No. 1007, *Paleoclimate Modeling Intercomparison Project (PMIP), proceedings of the third PMIP Workshop*, 2000.

Wohlfart, J., S. P. Harrison, and al., Synergistic feedbacks between ocean and vegetation on mid- and high latitude climates during the mid-holocene, *Climate Dynamics*, *22*, 223–238, 2004.

Zhao, Y., P. Braconnot, O. Marti, S. P. Harrison, C. Hewitt, A. Kitho, Z. Lui, U. Mikolajewicz, B. Otto-Bliesner, and S. L. Weber, A multi-model analysis of ocean feedback on the african and indian monsoon during the mid-Holocene, *in revision*, 2005.

List of Tables

List of Figures